Conformal Prediction in The Loop: A Feedback-Based Uncertainty Model for Trajectory Optimization

Han Wang

School of Automation and Intelligent Sensing Shanghai Jiao Tong University Shanghai 200240, China h.wang@sjtu.edu.cn

Chao Ning*

School of Automation and Intelligent Sensing Shanghai Jiao Tong University Shanghai 200240, China chao.ning@sjtu.edu.cn

Abstract

Conformal Prediction (CP) is a powerful statistical machine learning tool to construct uncertainty sets with coverage guarantees, which has fueled its extensive adoption in generating prediction regions for decision-making tasks, e.g., Trajectory Optimization (TO) in uncertain environments. However, existing methods predominantly employ a sequential scheme, where decisions rely unidirectionally on the prediction regions, and consequently the information from decision-making fails to be fed back to instruct CP. In this paper, we propose a novel Feedback-Based CP (Fb-CP) framework for shrinking-horizon TO with a joint risk constraint over the entire mission time. Specifically, a CP-based posterior risk calculation method is developed by fully leveraging the realized trajectories to adjust the posterior allowable risk, which is then allocated to future times to update prediction regions. In this way, the information in the realized trajectories is continuously fed back to the CP, enabling attractive feedback-based adjustments of the prediction regions and a provable online improvement in trajectory performance. Furthermore, we theoretically prove that such adjustments consistently maintain the coverage guarantees of the prediction regions, thereby ensuring provable safety. Additionally, we develop a decision-focused iterative risk allocation algorithm with theoretical convergence analysis for allocating the posterior allowable risk which closely aligns with Fb-CP. Furthermore, we extend the proposed method to handle distribution shift. The effectiveness and superiority of the proposed method are demonstrated through benchmark experiments.

1 Introduction

In recent years, Trajectory Optimization (TO) has recently garnered significant attention in the academic community Pan et al. [2024] and has achieved significant success in fields such as autonomous driving Zhou et al. [2020], autonomous surface vessels Tsolakis et al. [2024], and coverage control Davis et al. [2016]. However, collision-free TO in uncertain environments is a formidable challenge, because the intentions of obstacles are unknown. A crucial aspect of collision avoidance involves predicting obstacle trajectories. Existing trajectory prediction tools are unable to predict fully accurate trajectories. Therefore, a common approach is to generate the $(1-\alpha)$ -coverage prediction regions of the obstacle trajectories. If these regions contain the true trajectories with a probability of at least $1-\alpha$, they are considered *valid*. The key to probabilistic collision-free TO lies in adjusting the prediction regions while remaining valid to improve the trajectory performance.

Conformal Prediction (CP) is an attractive framework to produce prediction regions with finite-sample guarantees of validity Vovk et al. [2005], Shafer and Vovk [2008]. Without imposing any assumptions

^{*}Corresponding author.

about prediction algorithms and data distributions, CP utilizes a calibration dataset to obtain a valid prediction region for test data. Owing to its simplicity and versatility, CP and its variants have been widely applied in various safety-critical applications, such as probabilistic collision-free TO Lindemann et al. [2023], reliable estimation of graph neural networks H. Zargarbashi et al. [2023] and language modeling Quach et al. [2024].

However, there is a disconnect between existing research on CP theory and CP application for decision-making. On the side of CP theory, most existing work primarily focuses on upstream data, developing new CP algorithms to enhance prediction performance, such as addressing distributional shifts Gibbs and Candes [2021], performing multi-step time forecasting Sun and Yu [2023], and improving the efficiency of prediction regions Bai et al. [2022]. There is a lack of CP algorithms focused on enhancing the performance of downstream decisions. On the side of CP application for decision-making, most existing work embeds the CP into decision-making pipelines as a method for generating prediction regions, and employs a sequential approach, i.e. the prediction region is first computed using CP and then the decision depends unidirectionally on the prediction region without considering the favorable impact of the decision on the prediction region. However, this information channel blockage from the decision-making to the CP seriously prevents the CP from leveraging the information of past decisions to boost the performance of future decisions. Therefore, there is a pressing research need to develop a closed-loop framework that seamlessly integrates CP with decision-making, fully exploiting the information of past decisions to adjust prediction regions and thereby remarkably enhance the performance of future decisions.

To fill the aforementioned research gap, we propose a Feedback-Based CP (Fb-CP) framework for shrinking-horizon TO in uncertain environments and the collision risk over the total mission time is constrained at all times. The proposed framework leverages CP to construct the prediction regions of obstacle positions and adjusts these regions online in a closed-loop fashion while ensuring coverage guarantees, i.e. validity. In particular, we propose a novel posterior probability calculation method to obtain the posterior probability of collision conditional on realized trajectories. The posterior collision probability is then used to adjust the allowable collision risk, which is allocated to future times to yield prediction regions. In this manner, information from past trajectories is fed back to the CP through the posterior probability calculation, guiding the feedback-based adjustments of the prediction regions. Such adjustments in Fb-CP not only offer provable performance improvements but also consistently maintain the validity of the prediction regions. With the adjusted prediction regions, the trajectory is obtained by solving the resulting TO problem. Additionally, we further propose a decision-focused risk allocation method, i.e. Iterative Risk Allocation (IRA), which aims to optimize the trajectory performance by iteratively allocating the allowable risk to future times while enjoying the convergence guarantee. We highlight the main contributions of our work below.

- We propose, for the first time in the literature Fb-CP, a general uncertainty quantification framework closely associated with downstream decision-making which enables the adjustment of prediction regions using the feedback information embedded in decisions.
- We prove that 1) the feedback-based adjustments in Fb-CP do not compromise the coverage guarantees of prediction regions, and 2) Fb-CP offers guarantees for decision-making performance improvement. In other words, Fb-CP enjoys both validity and superior performance.
- We propose a decision-focused risk allocation algorithm with theoretical convergence analysis for Fb-CP, which optimizes the risk allocation to enhance decision-making performance.
- We extend Fb-CP to handle distribution shift by applying a weighting scheme to the test and calibration data and demonstrate its effectiveness.

2 Related work

Conformal Prediction. Conformal prediction originated in the early work Vovk et al. [1999, 2005], Shafer and Vovk [2008] to generate the prediction region. The salient advantage of CP lies in its ability to offer coverage guarantees regardless of prediction algorithms and data distributions. Most recently, various variants of CP have been developed to handle upstream data with different characteristics H. Zargarbashi et al. [2024], Liu et al. [2024] or to produce prediction regions in a wide array of forms Angelopoulos et al. [2024], Auer et al. [2023]. In response to the distribution shift in the upstream data, ACI Gibbs and Candes [2021], Podkopaev et al. [2024], Zaffran et al. [2022] and EnbPI Xu and Xie [2021, 2023] developed CP through online learning and sliding window,

respectively, and achieved asymptotic validity. In the context of multi-step time series forecasting, Sun and Yu [2023] combined CP with copula to propose the CopulaCPTS, while Cleaveland et al. [2024] employed an optimization-based method. Zhou et al. [2024b] presented a new conformal method for time series forecasting. In addition, numerous studies focused on improving the efficiency of the prediction region by changing the region shape Xu et al. [2024], minimizing the region length Kiyani et al. [2024], or optimizing the region construction function Bai et al. [2022]. Note that the prediction regions are typically utilized by downstream tasks in a sequential manner. However, the above research work primarily aims to enhance the predictive performance of CP rather than directly improving the performance of downstream decision-making.

Decision-making with CP. Many studies have focused on the integration of CP with decision-making. Vovk and Bendtsen [2018] was the first to the method of CP to make it applicable to decision-making. Additionally, Fannjiang et al. [2022] proposed a CP with coverage guarantee under one-step Feedback Covariate Shift (FCS), in which the test data depend on the training data. Building upon the aforementioned work, Prinster et al. [2024] refined its theoretical framework and extended it to multistep FCS. Furthermore, Lekeufack et al. [2024] introduced a conformal decision theory, which follows the ACI concept to directly provide provable statistical guarantees of having low risk for decisions made based on uncertainty-aware predictions.

TO using CP. Lindemann et al. [2023] and Strawn et al. [2023] applied CP to the safe planning for single-robot systems, while Muthali et al. [2023] and Kuipers et al. [2024] extended it to multi-robot systems. Additionally, Dixit et al. [2023] and Zhou et al. [2024a] employed the ACI to address the obstacle trajectory distribution shift. Stamouli et al. [2024] proposed a novel nonconformity score for shrinking-horizon TO. All the above methods directly employ CP in a sequential way to generate prediction regions. Nevertheless, the performance of realized trajectories has yet to be conveyed to the upstream CP as feedback information to adjust the prediction regions, which has the great potential to further boost the performance of trajectory.

3 Problem formulation and background

3.1 Problem formulation

Consider a discrete-time nonlinear dynamics as follows.

$$x_{t+1} = f(x_t, u_t), \quad x_0 = x_{init}$$
 (1)

where $x_t \in \mathcal{X} \subseteq \mathbb{R}^{n_x}$ and $u_t \in \mathcal{U} \subseteq \mathbb{R}^{n_u}$ are the state and control at time t=0,...,T, respectively, and $T \geq 1$ is the total mission time. The sets \mathcal{U} and \mathcal{X} represent the admissible sets of control inputs and system states, respectively. The function $f: \mathbb{R}^{n_x} \times \mathbb{R}^{n_u} \to \mathbb{R}^{n_x}$ represents the system dynamics and x_{init} is the initial state. For brevity, let $x_{t_1:t_2} := (x_{t_1},...,x_{t_2})$ and $u_{t_1:t_2} := (u_{t_1},...,u_{t_2})$ denote the state and control sequences from t_1 to t_2 , respectively. The system operates in an environment with M dynamic obstacles with a priori unknown trajectories. Let $Y_t := (Y_{t,1},...,Y_{t,M})$ represent the joint obstacle state at time t, where $Y_{t,j} \in \mathbb{R}^{n_p}$ denotes the state of obstacle j at time t. The dynamic of the above joint obstacle system can be expressed as follows.

$$Y_{t+1} = g(Y_{t-h}, ..., Y_{t-1}) + \omega_t \tag{2}$$

where h is the window length, $g(\cdot)$ represents the model learned from the historical data of the obstacle using machine learning tool, i.e., Long Short-Term Memory (LSTM). Naturally, readers may choose to adopt more powerful predictors for improved accuracy, such as Salzmann et al. [2020], Yuan et al. [2021], Salzmann et al. [2023], Yuan and Kitani [2020]. ω_t captures the modeling error. Additionally, we define $Y:=(Y_0,...,Y_T)$ as the entire trajectories of the obstacles, which is generated by sampling the initial state Y_0 from an unknown probability distribution $\mathcal D$ and by evolving it based on the dynamics (2). The system can observe the joint obstacle states $Y_0,...,Y_t$, when making the decision at time t. We assume the availability of an offline dataset as follows.

Assumption 3.1 We have a calibration dataset $D_{cal} := \{Y^{(1)}, ..., Y^{(N)}\}$, where each of the N joint obstacle trajectories is generated by independently sampling an initial state $Y_0^{(i)}$ from \mathcal{D} and evolving it based on its ground truth dynamics.

With Assumptions 3.1, we can conclude that the real joint obstacle trajectory Y and the N available joint obstacle trajectories $Y^{(i)}$ are independently and identically distributed (i.i.d.), and are also

exchangeable. Assumption 3.1 is not restrictive in practice, e.g. the historical trajectories of obstacles. In Appendix G, we introduce an extension to address the case where a shift exists between the initial state distributions of calibration data and test data, and the error ω_t represents state-dependent noise rather than being i.i.d..

We focus on the TO problem whose objective is to find the sequences $x_{1:T}$ and $u_{0:T-1}$ that minimize the cost function $J(x_{1:T}, u_{0:T-1})$ subject to the dynamics and constraints. The TO is performed in a shrinking-horizon fashion, with the optimization problem at time t formulated as follows.

$$\min_{\substack{x_{t+1:T}, u_{t:T-1} \\ x_{\tau} \in \mathcal{X}, \\ u_{\tau} \in \mathcal{U}, \\ x_{\tau} \in \mathcal{X}}} J(x_{t+1:T}, u_{t:T-1}) = l_{T}(x_{T}) + \sum_{\tau=t}^{T-1} l_{\tau}(x_{\tau}, u_{\tau}) \tag{3a}$$

$$s.t. \quad x_{\tau+1} = f(x_{\tau}, u_{\tau}), \qquad \forall \tau = t, ..., T-1 \tag{3b}$$

$$x_{\tau} \in \mathcal{X}, \qquad \forall \tau = t+1, ..., T \tag{3c}$$

$$u_{\tau} \in \mathcal{U}, \qquad \forall \tau = t, ..., T-1 \tag{3d}$$

s.t.
$$x_{\tau+1} = f(x_{\tau}, u_{\tau}), \qquad \forall \tau = t, ..., T-1$$
 (3b)

$$x_{\tau} \in \mathcal{X}, \qquad \forall \tau = t+1, ..., T$$
 (3c)

$$u_{\tau} \in \mathcal{U}, \qquad \forall \tau = t, ... T - 1$$
 (3d)

$$\mathbb{P}\left\{\bigcap_{\tau=1}^{T} \{c(x_{\tau}, Y_{\tau}) \ge 0\}\right\} \ge 1 - \alpha \tag{3e}$$

where $\mathbb{P}\{X\}$ denotes the probability of event X, the constraint function $c:=\mathbb{R}^{n_x}\times\mathbb{R}^{n_p}\to\mathbb{R}$ is L-Lipschitz continuous, which can encode various tasks, such as collision avoidance. Due to the uncertainty of the joint obstacle state Y_{τ} , we impose the joint chance constraint (3e) with failure probability $\alpha \in (0,1)$ to ensure that the joint probability of satisfying the constraint over the total mission time is no less than $1-\alpha$. To ensure the initial feasibility of the TO problem, we assume that the initial state satisfies the constraint, i.e. $c(x_0, Y_0) \ge 0$, with probability 1.

3.2 Conformal prediction

In this subsection, we provide a brief introduction to the theoretical results for CP and refer readers to Angelopoulos and Bates [2021] for a thorough introduction. Given N+1 exchangeable random variables $R^{(0)}, R^{(1)}, ..., R^{(N)}$ which is usually referred to as the nonconformity score, CP aims to find a probabilistic upper bound for R based on $R^{(1)}, ..., R^{(N)}$ such that R is less than this upper bound with high probability. In practice, $R^{(0)}$ represents the test data point, while $R^{(1)}, ..., R^{(N)}$ denote the calibration dataset. Formally, the central idea behind CP is summarized in Lemma A.1 provided in Appendix A.1.

Feedback-based conformal prediction

The challenge in solving the TO problem (3) lies in the computation of the joint probability (3e). Existing literature predominantly employs a sequential way of using CP, i.e. the prediction regions of obstacle positions are first computed based on the failure probability α , and then the decision of TO depends one-way on the prediction regions. However, it is important to note that in the shrinkinghorizon TO framework, at time t the past decisions $x_{0:t}$ are available and typically contain rich information that can instrumentally assist in refining the prediction regions at subsequent time steps, thereby considerably improving the performance of TO. Therefore, we propose a novel Feedbackbased Conformal Prediction (Fb-CP). Fb-CP not only exploits the feedback information provided by realized trajectories to perform closed-loop adjustments of the prediction regions but also maintains coverage guarantees. To begin with, the joint chance constraint (3e) can be reformulated as a set of individual chance constraints and a total risk constraint by using Boole's inequality as follows.

$$\mathbb{P}\left\{\bigcap_{\tau=1}^{T} \{c(x_{\tau}, Y_{\tau}) \ge 0\}\right\} \ge 1 - \alpha \Longleftrightarrow \left\{\begin{array}{l} \mathbb{P}\left\{c(x_{\tau}, Y_{\tau}) \ge 0\right\} \ge 1 - \alpha_{\tau}, \ \forall \tau = 1, ..., T\\ \sum_{\tau=1}^{T} \alpha_{\tau} \le \alpha \end{array}\right.$$
(4)

The risk α_T at each time can be initially allocated uniformly at time t=0, i.e. $\alpha_T=\alpha/T$, and remains constant throughout the shrinking-horizon TO process, as in Lindemann et al. [2023]. However, at time t, the system states x_{τ} for $\tau \leq t$ are available, which grants us to compute the posterior probability $\beta_{\tau} = \mathbb{P}\left\{c(x_{\tau}, Y_{\tau}) > 0 | x_{\tau}\right\}$ and the permissible risk for future times, which is then used to adjust the prediction regions. Using the information in the realized trajectories, the feedback-based adaptation of the prediction regions tremendously reduces the conservatism of trajectory online while ensuring coverage guarantees. In Subsection 4.1, we present the individual chance constraint reformulation using the prediction regions derived. In Subsection 4.2, we present a CP-based method for calculating β_{τ} . We reformulate the TO problem in Subsection 4.3.

4.1 Constraint reformulation using conformal prediction region

We randomly divide the calibration dataset D_{cal} into two subsets D_{cal}^1 and D_{cal}^2 with K and L joint obstacle trajectories, respectively, where K+L=N. Without loss of generality, we reassign indices to the joint obstacle trajectories as $D_{cal}^1:=\{Y^{(1)},...,Y^{(K)}\}$ and $D_{cal}^2:=\{Y^{(K+1)},...,Y^{(K+L)}\}$. At time t, we can obtain the prediction of the joint obstacle state $\hat{Y}_{\tau|t}$ for all future time $\tau=t+1,...,T$ using $g(\cdot)$ described in (2). Similarly, the prediction $\hat{Y}_{\tau|t}^{(i)}$ for each trajectory $Y^{(i)}$ in D_{cal}^1 is derived by using the same method. We define the nonconformity score as follows.

$$R_{\tau|t} = \|Y_{\tau} - \hat{Y}_{\tau|t}\|, \quad R_{\tau|t}^{(i)} = \|Y_{\tau}^{(i)} - \hat{Y}_{\tau|t}^{(i)}\| \quad \forall i = 1, ..., K$$
 (5)

Note that $Y_{\tau}, Y_{\tau}^{(1)}, ..., Y_{\tau}^{(K)}$ are exchangeable and the prediction function $g(\cdot)$ is trained from D_{train} independent of D_{cal}^1 . Therefore, given an allocated risk α_{τ} for future time τ , the random variables $R_{\tau|t}, R_{\tau|t}^{(1)}, ..., R_{\tau|t}^{(K)}$ are exchangeable and the prediction region with coverage guarantee is derived according to Lemma A.1 as follows.

$$\mathbb{P}\{\|Y_{\tau} - \hat{Y}_{\tau|t}\| \le C_{\tau|t}^{1-\alpha_{\tau}}\} \ge 1 - \alpha_{\tau} \tag{6a}$$

$$C_{\tau|t}^{1-\alpha_{\tau}} = Quantile_{1-\alpha_{\tau}}(R_{\tau|t}^{(1)}, ..., R_{\tau|t}^{(K)}, \infty)$$
 (6b)

Based on the $(1 - \alpha_{\tau})$ -coverage prediction region $\{y : \|y - \hat{Y}_{\tau|t}\| \le C_{\tau|t}^{1-\alpha_{\tau}}\}$, the individual chance constraint in (4) can be reformulated as the following lemma proven in Appendix B.1.

Lemma 4.1 (chance constraint) If Assumption 3.1 holds, the constraint function c is L-Lipschitz continuous and $c(x_{\tau}, \hat{Y}_{\tau|t}) \geq LC_{\tau|t}^{1-\alpha_{\tau}}$ is satisfied where $C_{\tau|t}^{1-\alpha_{\tau}}$ is calculated by (6b), then the individual chance constraint $\mathbb{P}\{c(x_{\tau}, Y_{\tau}) \geq 0\} \geq 1 - \alpha_{\tau}$ is satisfied.

For a general collision avoidance chance constraint of the form $\mathbb{P}\{\|x_{\tau}-Y_{\tau}\|-r\geq 0\}\geq 1-\alpha_{\tau}$, Lemma 4.1 effectively converts it into a deterministic constraint that requires the distance between x_{τ} and the predicted location $\hat{Y}_{\tau|t}$ to exceed the inflated radius derived from the prediction error, i.e., $\|x_{\tau}-Y_{\tau}\|-r-C_{\tau|t}^{1-\alpha_{\tau}}\geq 0$.

4.2 Posterior probability conditional on past decisions

At time t, the states x_{τ}^* for all past time $\tau=1,...,t$ are deterministic and available to the trajectory optimizer. We assume that x_{τ}^* is the true system state at time τ . Note that x_{τ}^* is a feasible solution to the TO problem (3) at time $\tau-1$ with the reformulated constraints through Lemma 4.1. Therefore, the individual chance constraint $\mathbb{P}\{c(x_{\tau}^*,Y_{\tau})\geq 0\}\geq 1-\alpha_{\tau}$ is satisfied at time $\tau-1$ and will be naturally satisfied for all time $\tau'\geq \tau-1$. However, the constraint violation probability α_{τ} is a priori probability allocated before time τ that tends to overstimate the violation probability and thus leads to conservative results. Fortunately, the determined x_{τ}^* allows us to compute the posterior probability of constraint violation β_{τ} , which, as we theoretically prove, is less than α_{τ} with high probability. The risk redundancy between α_{τ} and β_{τ} can be allocated across future times. In this way, the information embedded in x_{τ}^* is fed back from the decision-making to the CP to readjust the prediction region and to achieve a trajectory with notably improved performance. To compute β_{τ} using Lemma A.1, we propose a novel nonconformity score as follows.

$$S_{\tau} = c(x_{\tau}^*, \hat{Y}_{\tau|\tau-1} + \omega_{\tau}) = c(x_{\tau}^*, Y_{\tau}), \quad S_{\tau}^{(i)} = c(x_{\tau}^*, \hat{Y}_{\tau|\tau-1} + \omega_{\tau}^{(i)}) \quad \forall i = 1, ..., K + L \quad (7)$$

where $\omega_{\tau}^{(i)}$ is the modeling error of the joint obstacle trajectory $Y^{(i)}$ at time τ , which can be obtained through $\omega_{\tau}^{(i)} = Y_{\tau}^{(i)} - g(Y_{\tau-1}^{(i)})$. We note that $\omega_{\tau}, \omega_{\tau}^{(1)}, ..., \omega_{\tau}^{(K+L)}$ are i.i.d., and if x_{τ}^* is fixed and independent of $\omega_{\tau}, \omega_{\tau}^{(1)}, ..., \omega_{\tau}^{(K+L)}$, the random variables $S_{\tau}, S_{\tau}^{(1)}, ..., S_{\tau}^{(K+L)}$ are also exchangeable. However, as x_{τ}^* is derived through the TO problem (3) at time $\tau-1$, it depends on D_{cal}^1 and the random variables $S_{\tau}, S_{\tau}^{(1)}, ..., S_{\tau}^{(K)}$ are no longer exchangeable. Therefore, we only use the subset D_{cal}^2 , i.e. $S_{\tau}^{(K+1)}, ..., S_{\tau}^{(K+L)}$, to compute β_{τ} . The upper bound of the posterior violation probability β_{τ} is computed via the following lemma, whose proof is given in Appendix B.2.

Lemma 4.2 (posterior probability calculation) Assume that x_{τ}^* is the true state of the system at time τ , then the upper bound of the posterior violation probability at time τ is as follows.

$$\mathbb{P}\{c(x_{\tau}^*, Y_{\tau}) < 0\} \le \beta_{\tau} = \left(1 + \sum_{i=1}^{L} \mathbb{I}\left(S_{\tau}^{(K+i)} < 0\right)\right) / (1+L)$$
(8)

where $\mathbb{I}(\cdot)$ is the indicator function.

Lemma 4.2 essentially computes the posterior probability by evaluating the fraction of calibration set D_{cal}^2 samples whose actual trajectories would collide with the given realized position x_{τ}^* . Some might raise the concern that β_{τ} could be higher than α_{τ} , which could result in a more conservative trajectory when using β_{τ} in subsequent times. However, we can restrict the upper bound of the expectation of β_{τ} in Corollary A.2 provided in Appendix A.2. Additionally, we report the empirical observation that our method consistently tends to improve performance in practice, which is further discussed in Remark A.3 provided in Appendix A.2.

Optimization problem reformulation

By making use of the joint chance constraint reformulation (4), the individual constraint reformulation in Lemma 4.1 and the posterior probability in Lemma 4.2, the TO (3) is transformed as follows.

$$\min_{x_{t+1:T}, u_{t:T-1}, \alpha_{t+1:T}} J(x_{t+1:T}, u_{t:T-1}) = l_T(x_T) + \sum_{\tau=t}^{T-1} l_{\tau}(x_{\tau}, u_{\tau})$$

$$s.t. (3b) - (3d)$$
(9a)

$$s.t. (3b) - (3d)$$
 (9b)

$$c(x_{\tau}, \hat{Y}_{\tau|t}) \ge LC_{\tau|t}^{1-\alpha_{\tau}}, \quad \forall \tau = t+1, ..., T$$

$$\alpha_{\tau} \ge 0, \qquad \forall \tau = t+1, ..., T$$
(9c)
$$(9d)$$

$$\alpha_{\tau} > 0, \qquad \forall \tau = t + 1, ..., T$$
 (9d)

$$\alpha_{\tau} \ge 0, \qquad \forall \tau = t+1, ..., T$$

$$\sum_{\tau=t+1}^{T} \alpha_{\tau} \le \alpha - \sum_{\tau=0}^{t} \beta_{\tau}$$
(9d)
(9e)

where Constraint (9c) ensures the satisfaction of individual chance constraints (4) for future times $\tau=t+1,...,T$ through Lemma 4.1, and $C_{\tau}^{1-\alpha}$ is calculated by (6b). Constraint (9d) is imposed to ensure the non-negativity of α_{τ} . Constraint (9e) is the most important part for feedback-based adjustments of the prediction region and online performance enhancement of the optimized trajectory. It is derived by replacing α_{τ} for past time $\tau=1,...,t$ in the total risk constraint (4) with β_{τ} calculated through Lemma 4.2. The information embedded in past decisions $x_1^*, ..., x_t^*$ influences the future values of $\alpha_{t+1},...,\alpha_T$ through the calculation of $\beta_1,...,\beta_t$ thereby reshaping the prediction region of CP in an end-to-end way. Based on Corollary A.2 and Remark A.3, β_{τ} is highly likely to be less than α_{τ} in practice. Consequently, using β_{τ} grants more risk to be reserved for future times, resulting in much compact prediction regions and tremendously improved optimization performance.

However, it is important to note that $C_{\tau|t}^{1-\alpha_{\tau}}$ depends on α_{τ} and D_{cal}^{1} . Consequently, treating $\alpha_{t+1:T}$ as decision variables alongside $x_{t+1:T}$ and $u_{t:T-1}$ would make the optimization problem (9) computationally demanding to solve for larger values of T and K. Therefore, we will present an allocation method for $\alpha_{t+1:T}$ that aligns with the optimization problem (9) in the next section.

Shrinking-horizon trajectory optimization using Fb-CP

The shrinking-horizon TO framework using Fb-CP is illustrated in Figure 1. The information in $x_{0:t}^*$ guides the feedback-based adjustments of the size of the prediction regions $C_{\tau|t}^{1-\alpha_{\tau}}$ through posterior probability calculations. Solving the TO problem (9) is divided into two steps: 1) risk allocation and 2) TO with the fixed $\alpha_{t+1:T}$. The TO problem (9) with the fixed $\alpha_{t+1:T}$ is formalized as follows.

$$\min_{x_{t+1:T}, u_{t:T-1}} J(x_{t+1:T}, u_{t:T-1}) \quad s.t.(9b) - (9c) \tag{10}$$

The problem (10) can be readily solved to obtain $x_{t+1:T}^*$ and $u_{t:T-1}^*$ and only the first system input u_t^* is implemented as the control input. Therefore, as the actual time t progresses, the optimization horizon gradually shrinks. For the risk allocation, a general approach is the Average-based Risk Allocation (ARA), i.e. the allocable risk is evenly allocated across future times at time t below.

$$\alpha_{\tau} = (\alpha - \sum_{\tau=0}^{t} \beta_{\tau})/(T - t) \ \forall \tau = t + 1, ..., T$$
 (11)

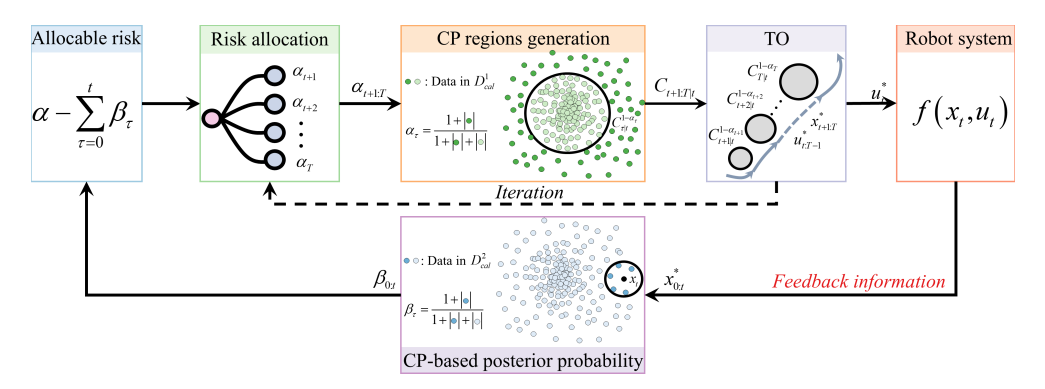


Figure 1: Shrinking-horizon trajectory optimization framework using Fb-CP.

Although the ARA method has the advantage of computational efficiency, the fixed proportion allocation significantly diminishes the flexibility in modifying the prediction regions for future times. Therefore, we extend the IRA Ono and Williams [2008] to the Fb-CP. We refer to the TO problem with the fixed $\alpha_{t+1:T}$ (10) and the risk allocation problem as the lower-stage and the upper-stage problem, respectively. The system states $x^*_{t+1:T}$ and inputs $u^*_{t:T-1}$, as well as the risk allocation $\alpha_{t+1:T}$ are obtained by iteratively solving the lower and upper-stage problems. We denote the feasible region of (10) with fixed $\alpha_{t+1:T}$ as $\mathcal{R}_t(\alpha_{t+1:T})$. The upper-stage problem is formally stated below.

$$\min_{\alpha_{t+1:T}} J^*(\alpha_{t+1:T}) \tag{12a}$$

$$s.t.\alpha_{\tau} \ge 0, \qquad \forall \tau = t+1,...,T$$
 (12b)

$$s.t.\alpha_{\tau} \ge 0, \qquad \forall \tau = t+1,...,T$$

$$\sum_{\tau=t+1}^{T} \alpha_{\tau} \le \alpha - \sum_{\tau=0}^{t} \beta_{\tau}$$
(12b)
$$(12c)$$

$$\sum_{\tau=t+1} \alpha_{\tau} \le \alpha - \sum_{\tau=0} \beta_{\tau}$$

$$\alpha_{t+1:T} \in \{\alpha_{t+1:T} : \exists (x, u) \in \mathcal{R}_t(\alpha_{t+1:T})\}$$
(12d)

where $J^*(\alpha_{t+1:T})$ is the optimal objective function of (10) given $\alpha_{t+1:T}$. If a risk allocation $\alpha_{t+1:T}$ satisfies (12b)-(12d), then we refer to $\alpha_{t+1:T}$ a feasible risk allocation. However, the lower-stage problem (12) is challenging to solve due to the computational complexity arising from its objective (12a) and Constraint (12c). To solve (12) efficiently, we introduce a descent algorithm, i.e. IRA for Fb-CP which is based on the monotonicity of $J^*(\alpha_{t+1:T})$ below, which is proven in Appendix B.4.

Lemma 5.1 (monotonicity of J^*) At time t, the following inequalities always hold.

$$\frac{\partial J^*(\alpha_{t+1:T})}{\partial \alpha_{\tau}} \le 0 \quad \forall \tau = t+1, ..., T \tag{13}$$

The monotonicity of J^* in Lemma 5.1 shows that increasing the allocated risk α_{τ} at any time step will strictly decrease the optimal cost of the trajectory optimizer. This insight enables our risk reallocation strategy: by reducing redundant risk at inactive time steps and reallocating it to active ones, we can lower the overall optimal cost.

We assume that $\alpha_{t+1:T}^n$ represents the feasible risk allocation obtained after the nth iteration at time t. IRA aims to obtain a feasible risk allocation $\alpha_{t+1:T}^{n+1}$ in the (n+1)th iteration such that $J^*(\alpha_{t+1:T}^{n+1}) \leq 1$ $J^*(\alpha^n_{t+1:T})$. In the (n+1)th iteration, IRA first solves the lower-stage problem (10) using $\alpha^n_{t+1:T}$ to obtain the optimal solution $x_{t+1:T}^n$ and $u_{t:T-1}^n$. Subsequently, based on $x_{t+1:T}^n$, Constraint (9c) in the lower-stage problem (10) is categorized into active and inactive constraints. The active and inactive constraint sets are formally defined as $\mathcal{I}_{act} := \{\tau: c(x_{\tau}^n, \hat{Y}_{\tau|t}) = LC_{\tau|t}^{1-\alpha_{\tau}^n}, \ \tau = t+1, ..., T\}$ and $\mathcal{I}_{ina} := \{ \tau : \tau \notin \mathcal{I}_{act}, \ \tau = t+1,...,T \}$, respectively. In summary, IRA consists of two steps: 1) tightening the inactive constraints and 2) relaxing the active constraints.

Tightening the inactive constraints is first implemented to construct $\widetilde{\alpha}_{t+1:T}^n$ from $\alpha_{t+1:T}^n$. Specifically, for $\tau \in \mathcal{I}_{act}$, set $\widetilde{\alpha}_{\tau}^n = \alpha_{\tau}^n$. Based on the definition of $C_{\tau|t}^{1-\alpha_{\tau}}$ (6b), $C_{\tau|t}^{1-\alpha_{\tau}}$ is non-increasing with respect to α_{τ} for the fixed D_{cal}^1 . Thus for $\tau \in \mathcal{I}_{ina}$, we choose $\widetilde{\alpha}_{\tau}^n \leq \alpha_{\tau}^n$ so that

$$c(x_{\tau}^n, \hat{Y}_{\tau|t}) \ge LC_{\tau|t}^{1-\tilde{\alpha}_{\tau}^n} \ge LC_{\tau|t}^{1-\alpha_{\tau}^n}$$

$$\tag{14}$$

Based on (14), it can be deduced that $(x^n_{t+1:T}, u^n_{t:T-1}) \in \mathcal{R}_t(\widetilde{\alpha}^n_{t+1:T}) \subseteq \mathcal{R}_t(\alpha^n_{t+1:T})$. Therefore, the optimal solution $(x^n_{t+1:T}, u^n_{t:T-1})$ for $\alpha^n_{t+1:T}$ is also the optimal solution for $\widetilde{\alpha}^n_{t+1:T}$, and thus $J^*(\alpha^n_{t+1:T}) = J^*(\widetilde{\alpha}^n_{t+1:T})$. Finally, it is straightforward to show that $\widetilde{\alpha}^n_{t+1:T}$ is a feasible risk allocation, because (i) (12b) follows from (14) and the fact that when $\alpha_\tau \to 0$, $C^{1-\alpha_\tau}_{\tau|t} \to \infty$; (ii) (12c) is satisfied since $\sum_{\tau=t+1}^T \widetilde{\alpha}^n_\tau \leq \sum_{\tau=t+1}^T \alpha^n_\tau \leq \alpha - \sum_{\tau=1}^t \beta_\tau$; (iii) (12d) is satisfied because $(x^n_{t+1:T}, u^n_{t:T-1})$ is feasible for $\widetilde{\alpha}_{t+1:T}$. The specific construction of $\widetilde{\alpha}^n_\tau$ is as follows.

$$\widetilde{\alpha}_{\tau}^{n} = \begin{cases} \alpha_{\tau}^{n}, & \tau \in \mathcal{I}_{act} \\ (1 - \eta)\alpha_{\tau}^{n} + \eta \underline{\alpha}_{\tau}^{n}, & \tau \in \mathcal{I}_{ina} \end{cases}$$
 (15)

where $\eta \in (0,1)$ is the step size and $\underline{\alpha}_{\tau}^{n}$ is the lower bound of $\widetilde{\alpha}_{\tau}^{n}$ calculated as in Lemma 5.2.

Lemma 5.2 (constraint tightening) Assume that $x_{t+1:T}^n$ is feasible for the problem (10) with $\alpha_{t+1:T}^n$ and $\alpha_{t+1:T}^n < 1$. For $\tau \in \mathcal{I}_{ina}$, the lower bound of $\widetilde{\alpha}_{\tau}^n$ while satisfying (14) is as follows.

$$\underline{\alpha}_{\tau}^{n} = \left(1 + \sum_{i=1}^{K} \mathbb{I}\left(c(x_{\tau}^{n}, \hat{Y}_{\tau|t}) < LR_{\tau|t}^{(i)}\right)\right) / (1 + K)$$

$$(16)$$

Furthermore, it is deterministic that $\underline{\alpha}_{\tau}^{n} \leq \alpha_{\tau}^{n}$.

Lemma 5.2 is proven in Appendix B.5. Then $\alpha_{t+1:T}^{n+1}$ is constructed from $\widetilde{\alpha}_{t+1:T}^n$ to relax the active constraints as follows.

$$\alpha_{\tau}^{n+1} = \begin{cases} \widetilde{\alpha}_{\tau}^{n} + (\alpha - \sum_{\tau=1}^{t} \beta_{\tau} - \sum_{\tau=t+1}^{T} \widetilde{\alpha}_{\tau}^{n}) / N_{act}, & \tau \in \mathcal{I}_{act} \\ \widetilde{\alpha}_{\tau}^{n}, & \tau \in \mathcal{I}_{ina} \end{cases}$$
(17)

where N_{act} represents the number of elements in the set \mathcal{I}_{act} . It can be easily verified that $\alpha_{t+1:T}^{n+1}$ satisfies (12b)-(12d), and thus $\alpha_{t+1:T}^{n+1}$ is a feasible risk allocation. Note that $\alpha_{\tau}^{n+1} \geq \widetilde{\alpha}_{\tau}^{n}$ since $\widetilde{\alpha}_{\tau}^{n}$ satisfies (12c). Therefore, the following inequality is obtained by implying Lemma 5.1.

$$J^*(\alpha_{t+1:T}^{n+1}) \le J^*(\widetilde{\alpha}_{t+1:T}^n) = J^*(\alpha_{t+1:T}^n)$$
(18)

By recursively constructing $\alpha_{t+1:T}^1, ..., \alpha_{t+1:T}^n$ in this manner, J^* monotonically decreases. The algorithm of Fb-CP using IRA at time t isis delineated in Algorithm 5. Note that at time t=0, the input parameter $\alpha_{0:T}$ is initialized and ϵ is a given small tolerance. At time t, the robot first obtains x_t and Y_t (Line 2). Then, based on $Y_0, ... Y_t$, the future joint obstacle states $\hat{Y}_{t+1|T}, ..., \hat{Y}_{T|t}$ are predicted using LSTMs (Line 3). Additionally, based on x_t and D^2_{cal} , the posterior collision risk can be calculated through (8) (Line 4). After initialization (Line 5), IRA jointly optimizes risk allocation and trajectory through iteration (Line 6-12). Specifically, in each iteration, IRA first computes the optimal control $u^n_{t:T-1}$, state $x^n_{t+1:T}$, and cost $J^*(\alpha^n_{t+1:T})$ for the current iteration based on the risk allocation $\alpha^n_{t+1:T}$ obtained from the previous iteration (Line 7). The active and inactive constraint sets \mathcal{I}_{act} , \mathcal{I}_{ina} are determined based on the optimal state $x^n_{t+1:T}$ (Line 8). And then, by sequentially applying the inactive constraint tightening (15) (Line 9) and the redundant risk reallocation (17) (Line 10), the updated risk allocation $\alpha^{n+1}_{t+1:T}$ is obtained. Finally, if the convergence condition is satisfied, the the optimal control $u^n_{t:T-1}$ and the risk allocation $u^{n-1}_{t+1:T}$ are output; otherwise, the next iteration begins (Line 12). Finally, the convergence of Algorithm 5 and the overall risk guarantee are established in Theorems 5.3 and 5.4, whose proofs are provided in Appendices B.6 and B.7, respectively.

Theorem 5.3 (convergence guarantee) Assume that $x_{t+1:T}^0$, $u_{t:T-1}^0$ are feasible in problem (10) with risk allocation $\alpha_{t+1:T}^0$. If the sets \mathcal{X} , \mathcal{U} are bounded and the objective function $J(x_{t+1:T}, u_{t:T-1})$ is continuous, then the sequence of the optimal objective $\{J^*(\alpha_{t+1:T}^n)\}_{n\in\mathbb{N}}$ converges to a finite limit.

Theorem 5.4 (overall risk guarantee for entire trajectory) Given an overall risk tolerance α , if the posterior risk $\beta_{1:t}$ is calculated through Lemma 4.2, the risk $\alpha_{t+1:T}$ is allocated through ARA (11) or IRA (12), the planned state $x_{t+1:T}^*$ is a feasible solution of the TO problem (10) with $\alpha_{t+1:T}$, then the entire trajectory at time t satisfies the overall risk guarantee $\mathbb{P}\{\bigcap_{\tau=1}^T \{C(x_{\tau}^*, Y_{\tau}) \geq 0\}\} \geq 1 - \alpha$.

Remark 5.5 One may notice that the calculation of β_{τ} in Lemma 4.2 is similar to the computation of $\widetilde{\alpha}_{\tau}^n$ in Lemma 5.2. This observation is correct. The key difference between the two lies in that the former utilizes the dataset D_{cal}^2 independent with D_{cal}^1 to achieve the coverage guarantee for β_{τ} . By contrast, as a step in solving (11), the latter does not need to consider the coverage guarantee and thus directly uses D_{cal}^1 . The use of different datasets results in the former providing probabilistic guarantee, while the latter achieves deterministic guarantee $(\underline{\alpha}_{\tau}^n \leq \alpha_{\tau}^n)$.

Algorithm 1 Fb-CP using IRA at time t

```
1: Input: \alpha, \alpha_{t:T}, \beta_{0:t-1}, \epsilon, \eta, D_{cal}^1, D_{cal}^2

2: Observe the system state x_t and joint obstacle states Y_t

3: \hat{Y}_{t+1|t}, ..., \hat{Y}_{T|t} \leftarrow Trajectory prediction using LSTMs based on Y_0, ..., Y_t

4: \beta_t \leftarrow Posterior probability calculation (8) {Using x_t and D_{cal}^2}

5: J^*(\alpha_{t+1:T}^{-1}) \leftarrow \infty, \alpha_{t+1:T}^0 \leftarrow \alpha_{t+1:T}, n \leftarrow 0 {Initialization of IRA}

6: repeat

7: J^*(\alpha_{t+1:T}^n), x_{t+1:T}^n, u_{t:T-1}^n \leftarrow Solve the lower-stage problem (10) with \alpha_{t+1:T}^n

8: \mathcal{I}_{act}, \mathcal{I}_{ina}, N_{act} \leftarrow Identification of active and inactive constraints

9: \widetilde{\alpha}_{t+1:T}^n \leftarrow Transitional risk allocation calculation (15)

10: \alpha_{t+1:T}^{n+1} \leftarrow New risk allocation calculation (17)

11: n \leftarrow n+1

12: until |J^*(\alpha_{t+1:T}^{n-1}) - J^*(\alpha_{t+1:T}^{n-2})| < \epsilon

13: Output: \beta_{0:t}, u_{t:T-1}^{n-1}, \alpha_{t+1:T} = \alpha_{t+1:T}^{n-1}
```

6 Experiments

All the experiments are performed on a personal computer with 2.10 GHz Inter Core i7-13700 CPU and 32 GB RAM. We conduct 1,000 Monte Carlo experiments on a kinematic vehicle model Lekeufack et al. [2024], a 3D linear quadrotor model Dixit et al. [2023], a dynamic bicycle model Hakobyan and Yang [2021] and the Stanford Drone Dataset Robicquet et al. [2016] to compare our method with the state-of-art methods as follows ².

- (i) Conformal Control (CC) proposed in Lekeufack et al. [2024].
- (ii) ACI for Motion Planning (ACI-MP) proposed in Dixit et al. [2023].
- (iii) Recursively Feasible MPC using CP (RF-CP) proposed in Stamouli et al. [2024]
- (iv) Sequential CP (S-CP) proposed in Lindemann et al. [2023].
- (v) Fb-CP with ARA (Fb-CP-ARA): The method based on Fb-CP using average risk allocation.
- (vi) Fb-CP with IRA (Fb-CP-IRA): The method based on Fb-CP using iterative risk allocation. In this section, we present the main experimental results, while the full set of results can be found in Appendix C. Figure 2 shows the simulation results from one of the 1,000 simulations using the 2D vehicle model. At t=0, the vehicle performs the first TO. For Fb-CP-IRA, IRA allows for flexible allocation of the risks across future times. Therefore, by assigning more risk to $\tau = 9$, which leads to a compact prediction region, a trajectory passing between Obstacles 2 and 3 is obtained. However, with the fixed risk allocation at t = 0, S-CP and Fb-CP-ARA can only optimize the trajectory based on fixed prediction regions. Consequently, they can only navigate around to pass between Obstacles 1 and 2. Note that at t=0, no deterministic vehicle position is available for posterior probability calculation. Thus Fb-CP-ARA degenerates into S-CP, resulting in both methods obtaining essentially the same trajectory. As time progresses, more and more vehicle positions become available. For Fb-CP-ARA, $\beta_{1:3}$ can be computed at t=3 and is with high probability less than $\alpha_{1:3}$, as outlined in Corollary A.2. The reduction from $\alpha_{1:3}$ to $\beta_{1:3}$ leads to an increased allowable risk for future times, corresponding to a narrowing in the prediction regions. Therefore, compared with S-CP, Fb-CP-ARA generates a less conservative trajectory. Similarly, Fb-CP-IRA also leverages $\beta_{1:3}$ to increase the total allocable risk, thereby further enhancing the flexibility in allocating risks. As shown in Figure 2, the trajectory obtained by Fb-CP-IRA at t=3 exhibits reduced conservativeness compared with the trajectory obtained at t = 0.

Table 1 summarizes the average cost, computation time, and collision avoidance rate of 1,000 simulations using the quadrotor model with different methods. As shown in Table 1, the Fb-CP-ARA reduces the cost by an average of 11.34% compared with S-CP thanks to the feedback information of posterior probabilities, with a negligible additional computational burden. Furthermore, by flexibly allocating the additional allowable risk provided by posterior probabilities, Fb-CP-IRA achieves an 58.50% reduction in average cost compared with S-CP. However, since IRA needs to solve the TO problem (10) iteratively, the average computation time increases significantly. Additionally, since CC and ACI-MP fail to fully utilize the information in the calibration dataset, they incur higher costs, which are 184% and 296% higher than those of Fb-CP-IRA, respectively. Particularly for CC, it directly controls the collision avoidance rate by adjusting the weight of the collision penalty term

²https://github.com/DOCU-Lab/Feedback-based_Conformal_Prediction

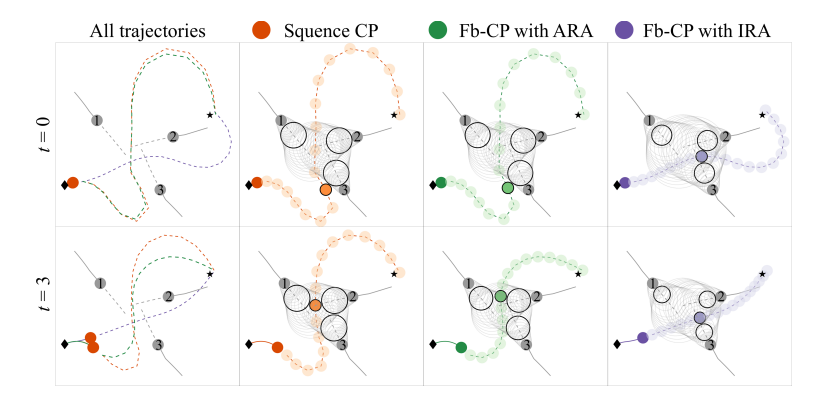


Figure 2: Trajectories of the vehicle with different TO methods. (Numbers on the circles denote the indices of obstacles. The diamond and pentagon symbols represent the initial and target points of the vehicle, respectively. The translucent circles represent the planned positions of the vehicle and the prediction regions for further time. In particular, the colored and transparent circles with black edges denote the planned positions and the prediction regions for $\tau = 9$, respectively.)

in the objective function, which results in a higher average cost. However, it should be noted that, in practice, CC and ACI-MP are better suited for scenarios where the test data exhibit distribution shift, rather than the setup considered in our work. For RF-CP, thanks to the proposed normalized nonconformity score, its average cost is comparable to that of Fb-CP-ARA, but it remains 85.8% higher than Fb-CP-IRA. However, the normalized nonconformity score introduces mixed-integer variables into the TO problem, significantly increasing the computation time. Specifically, the average computation time of RF-CP is more than an order of magnitude higher than that of Fb-CP-IRA.

Additionally, we have investigated the impact of using prior versus posterior probabilities on the prediction regions by analyzing the prediction region radius at different time t and τ in Appendix H. Furthermore, we have also extended Fb-CP to handle distribution shift and empirically demonstrate its effectiveness. Detailed methodology and corresponding experiments can be found in Appendix G.

Table 1: Average cost, computation time, and collision avoidance rate using the quadrotor model with different methods (η is the learning rate of CC).

| | CC | ACI-MP | RF-CP | S-CP | Fb-CP | | | |
|------------------|-------------------|--------|-----------------|--------|--------|--------|--------|-------|
| | | | | | | | ARA | IRA |
| | $\eta = 1000$ | 59.25 | $\alpha = 0.05$ | 17.970 | 15.794 | 17.321 | 15.356 | 7.189 |
| Average | $\eta = 500$ | 47.50 | $\alpha = 0.10$ | 17.263 | 14.378 | 16.17 | 14.228 | 6.798 |
| cost | $\eta = 100$ | 22.46 | $\alpha = 0.15$ | 16.096 | 11.922 | 14.83 | 12.354 | 6.191 |
| | $\eta = 50$ | 21.34 | $\alpha = 0.20$ | 15.310 | 10.032 | 13.217 | 10.22 | 5.398 |
| A | $\eta = 1000$ | 0.019 | $\alpha = 0.05$ | 0.022 | 0.487 | 0.022 | 0.027 | 0.038 |
| Average | $\eta = 500$ | 0.019 | $\alpha = 0.10$ | 0.026 | 0.494 | 0.020 | 0.021 | 0.039 |
| computation time | $\eta = 100$ | 0.021 | $\alpha = 0.15$ | 0.021 | 0.545 | 0.021 | 0.020 | 0.037 |
| ume | $\eta = 50$ | 0.022 | $\alpha = 0.20$ | 0.022 | 0.500 | 0.020 | 0.019 | 0.036 |
| Collision | $\eta = 1000$ | 97.0% | $\alpha = 0.05$ | 98.6% | 98.7% | 98.8% | 98.2% | 96.3% |
| | $\eta = 500$ | 92.8% | $\alpha = 0.10$ | 93.3% | 96.9% | 93.5% | 94.6% | 94.1% |
| avoidance | $\eta = 100$ | 82.5% | $\alpha = 0.15$ | 91.5% | 92.4% | 92.0% | 90.2% | 91.9% |
| rate | $\dot{\eta} = 50$ | 79.1% | $\alpha = 0.20$ | 87.9% | 90.0% | 88.2% | 86.7% | 88.2% |

7 Conclusion and Limitations

In this paper, we proposed a Fb-CP framework for shrinking-horizon TO with a joint risk constraint in uncertain environments. This method enables the feedback of the information in the realized trajectory from the decision-making to the CP, guiding the closed-loop adjustments of the prediction regions. The proposed adjustment rule balances both performance and safety, offering provable performance and coverage guarantees. The limitations are discussed in detail in Appendix L.

Acknowledgements

This work was supported in part by the National Natural Science Foundation of China under Grants 62473256 and 62103264.

References

- Alexandre Alahi, Kratarth Goel, Vignesh Ramanathan, Alexandre Robicquet, Li Fei-Fei, and Silvio Savarese. Social lstm: Human trajectory prediction in crowded spaces. In *Proceedings of the IEEE conference on computer vision and pattern recognition*, pages 961–971, 2016.
- Anastasios Angelopoulos, Emmanuel Candes, and Ryan J Tibshirani. Conformal pid control for time series prediction. *Advances in neural information processing systems*, 36, 2024.
- Anastasios N Angelopoulos and Stephen Bates. A gentle introduction to conformal prediction and distribution-free uncertainty quantification. *arXiv preprint arXiv:2107.07511*, 2021.
- Andreas Auer, Martin Gauch, Daniel Klotz, and Sepp Hochreiter. Conformal prediction for time series with modern hopfield networks. *Advances in Neural Information Processing Systems*, 36: 56027–56074, 2023.
- Yu Bai, Song Mei, Huan Wang, Yingbo Zhou, and Caiming Xiong. Efficient and differentiable conformal prediction with general function classes. *arXiv preprint arXiv:2202.11091*, 2022.
- Matthew Cleaveland, Insup Lee, George J Pappas, and Lars Lindemann. Conformal prediction regions for time series using linear complementarity programming. In *Proceedings of the AAAI Conference on Artificial Intelligence*, volume 38, pages 20984–20992, 2024.
- Bobby Davis, Ioannis Karamouzas, and Stephen J Guy. C-opt: Coverage-aware trajectory optimization under uncertainty. *IEEE Robotics and Automation Letters*, 1(2):1020–1027, 2016.
- Anushri Dixit, Lars Lindemann, Skylar X Wei, Matthew Cleaveland, George J Pappas, and Joel W Burdick. Adaptive conformal prediction for motion planning among dynamic agents. In *Learning for Dynamics and Control Conference*, pages 300–314. PMLR, 2023.
- Clara Fannjiang, Stephen Bates, Anastasios N Angelopoulos, Jennifer Listgarten, and Michael I Jordan. Conformal prediction under feedback covariate shift for biomolecular design. *Proceedings of the National Academy of Sciences*, 119(43):e2204569119, 2022.
- Isaac Gibbs and Emmanuel Candes. Adaptive conformal inference under distribution shift. *Advances in Neural Information Processing Systems*, 34:1660–1672, 2021.
- Soroush H. Zargarbashi, Simone Antonelli, and Aleksandar Bojchevski. Conformal prediction sets for graph neural networks. In *Proceedings of the 40th International Conference on Machine Learning*, volume 202, pages 12292–12318. PMLR, 2023.
- Soroush H. Zargarbashi, Mohammad Sadegh Akhondzadeh, and Aleksandar Bojchevski. Robust yet efficient conformal prediction sets. In *Proceedings of the 41st International Conference on Machine Learning*, volume 235, pages 17123–17147. PMLR, 2024.
- Astghik Hakobyan and Insoon Yang. Wasserstein distributionally robust motion control for collision avoidance using conditional value-at-risk. *IEEE Transactions on Robotics*, 38(2):939–957, 2021.
- Shayan Kiyani, George Pappas, and Hamed Hassani. Length optimization in conformal prediction. *arXiv preprint arXiv:2406.18814*, 2024.
- Parth Kothari, Sven Kreiss, and Alexandre Alahi. Human trajectory forecasting in crowds: A deep learning perspective. *IEEE Transactions on Intelligent Transportation Systems*, 23(7):7386–7400, 2021.
- Tom Kuipers, Renukanandan Tumu, Shuo Yang, Milad Kazemi, Rahul Mangharam, and Nicola Paoletti. Conformal off-policy prediction for multi-agent systems. *arXiv preprint arXiv:2403.16871*, 2024.

- Jordan Lekeufack, Anastasios N Angelopoulos, Andrea Bajcsy, Michael I Jordan, and Jitendra Malik. Conformal decision theory: Safe autonomous decisions from imperfect predictions. In 2024 IEEE International Conference on Robotics and Automation (ICRA), pages 11668–11675. IEEE, 2024.
- Lars Lindemann, Matthew Cleaveland, Gihyun Shim, and George J Pappas. Safe planning in dynamic environments using conformal prediction. *IEEE Robotics and Automation Letters*, 2023.
- Yi Liu, Alexander Levis, Sharon-Lise Normand, and Larry Han. Multi-source conformal inference under distribution shift. In *Proceedings of the 41st International Conference on Machine Learning*, volume 235, pages 31344–31382. PMLR, 2024.
- Anish Muthali, Haotian Shen, Sampada Deglurkar, Michael H Lim, Rebecca Roelofs, Aleksandra Faust, and Claire Tomlin. Multi-agent reachability calibration with conformal prediction. In 2023 62nd IEEE Conference on Decision and Control (CDC), pages 6596–6603. IEEE, 2023.
- Masahiro Ono and Brian C Williams. Iterative risk allocation: A new approach to robust model predictive control with a joint chance constraint. In 2008 47th IEEE Conference on Decision and Control, pages 3427–3432. IEEE, 2008.
- Chaoyi Pan, Zeji Yi, Guanya Shi, and Guannan Qu. Model-based diffusion for trajectory optimization. In *The Thirty-eighth Annual Conference on Neural Information Processing Systems*, 2024.
- Aleksandr Podkopaev, Dong Xu, and Kuang-chih Lee. Adaptive conformal inference by betting. In *Forty-first International Conference on Machine Learning*, 2024.
- Drew Prinster, Samuel Don Stanton, Anqi Liu, and Suchi Saria. Conformal validity guarantees exist for any data distribution (and how to find them). In *Forty-first International Conference on Machine Learning*, 2024.
- Victor Quach, Adam Fisch, Tal Schuster, Adam Yala, Jae Ho Sohn, Tommi S. Jaakkola, and Regina Barzilay. Conformal language modeling. In *The Twelfth International Conference on Learning Representations*, 2024.
- Alexandre Robicquet, Amir Sadeghian, Alexandre Alahi, and Silvio Savarese. Learning social etiquette: Human trajectory understanding in crowded scenes. In *European conference on computer vision*, pages 549–565. Springer, 2016.
- Tim Salzmann, Boris Ivanovic, Punarjay Chakravarty, and Marco Pavone. Trajectron++: Dynamically-feasible trajectory forecasting with heterogeneous data. In *European Conference on Computer Vision*, pages 683–700. Springer, 2020.
- Tim Salzmann, Hao-Tien Lewis Chiang, Markus Ryll, Dorsa Sadigh, Carolina Parada, and Alex Bewley. Robots that can see: Leveraging human pose for trajectory prediction. *IEEE Robotics and Automation Letters*, 8(11):7090–7097, 2023.
- Glenn Shafer and Vladimir Vovk. A tutorial on conformal prediction. *Journal of Machine Learning Research*, 9(3), 2008.
- Charis Stamouli, Lars Lindemann, and George Pappas. Recursively feasible shrinking-horizon mpc in dynamic environments with conformal prediction guarantees. In *6th Annual Learning for Dynamics & Control Conference*, pages 1330–1342. PMLR, 2024.
- Kegan J Strawn, Nora Ayanian, and Lars Lindemann. Conformal predictive safety filter for rl controllers in dynamic environments. *IEEE Robotics and Automation Letters*, 2023.
- Sophia Huiwen Sun and Rose Yu. Copula conformal prediction for multi-step time series prediction. In *The Twelfth International Conference on Learning Representations*, 2023.
- Ryan J Tibshirani, Rina Foygel Barber, Emmanuel Candes, and Aaditya Ramdas. Conformal prediction under covariate shift. *Advances in neural information processing systems*, 32, 2019.
- Anastasios Tsolakis, Rudy R Negenborn, Vasso Reppa, and Laura Ferranti. Model predictive trajectory optimization and control for autonomous surface vessels considering traffic rules. *IEEE Transactions on Intelligent Transportation Systems*, 2024.

- Vladimir Vovk. Conditional validity of inductive conformal predictors. In *Asian conference on machine learning*, pages 475–490. PMLR, 2012.
- Vladimir Vovk and Claus Bendtsen. Conformal predictive decision making. In *Conformal and Probabilistic Prediction and Applications*, pages 52–62. PMLR, 2018.
- Vladimir Vovk, Alexander Gammerman, and Glenn Shafer. *Algorithmic learning in a random world*, volume 29. Springer, 2005.
- Volodya Vovk, Alexander Gammerman, and Craig Saunders. Machine-learning applications of algorithmic randomness. 1999.
- Chen Xu and Yao Xie. Conformal prediction interval for dynamic time-series. In *International Conference on Machine Learning*, pages 11559–11569. PMLR, 2021.
- Chen Xu and Yao Xie. Sequential predictive conformal inference for time series. In *International Conference on Machine Learning*, pages 38707–38727. PMLR, 2023.
- Chen Xu, Hanyang Jiang, and Yao Xie. Conformal prediction for multi-dimensional time series by ellipsoidal sets. In *Proceedings of the 41st International Conference on Machine Learning*, volume 235, pages 55076–55099. PMLR, 2024.
- Ye Yuan and Kris M. Kitani. Diverse trajectory forecasting with determinantal point processes. In *International Conference on Learning Representations*, 2020.
- Ye Yuan, Xinshuo Weng, Yanglan Ou, and Kris M Kitani. Agentformer: Agent-aware transformers for socio-temporal multi-agent forecasting. In *Proceedings of the IEEE/CVF international conference on computer vision*, pages 9813–9823, 2021.
- Margaux Zaffran, Olivier Féron, Yannig Goude, Julie Josse, and Aymeric Dieuleveut. Adaptive conformal predictions for time series. In *International Conference on Machine Learning*, pages 25834–25866. PMLR, 2022.
- Hao Zhou, Yanze Zhang, and Wenhao Luo. Safety-critical control with uncertainty quantification using adaptive conformal prediction. In *2024 American Control Conference (ACC)*, pages 574–580. IEEE, 2024a.
- Jinyun Zhou, Runxin He, Yu Wang, Shu Jiang, Zhenguang Zhu, Jiangtao Hu, Jinghao Miao, and Qi Luo. Autonomous driving trajectory optimization with dual-loop iterative anchoring path smoothing and piecewise-jerk speed optimization. *IEEE Robotics and Automation Letters*, 6(2): 439–446, 2020.
- Yanfei Zhou, Lars Lindemann, and Matteo Sesia. Conformalized adaptive forecasting of heterogeneous trajectories. In *Proceedings of the 41st International Conference on Machine Learning*, volume 235, pages 62002–62056. PMLR, 21–27 Jul 2024b.
- Steve Zymler, Daniel Kuhn, and Berç Rustem. Distributionally robust joint chance constraints with second-order moment information. *Mathematical Programming*, 137:167–198, 2013.

NeurIPS Paper Checklist

1. Claims

Question: Do the main claims made in the abstract and introduction accurately reflect the paper's contributions and scope?

Answer: [Yes]

Justification: The main claims in the abstract and introduction clearly and accurately summarize the paper's core contributions and align well with the methods and results presented.

Guidelines:

- The answer NA means that the abstract and introduction do not include the claims made in the paper.
- The abstract and/or introduction should clearly state the claims made, including the
 contributions made in the paper and important assumptions and limitations. A No or
 NA answer to this question will not be perceived well by the reviewers.
- The claims made should match theoretical and experimental results, and reflect how much the results can be expected to generalize to other settings.
- It is fine to include aspirational goals as motivation as long as it is clear that these goals are not attained by the paper.

2. Limitations

Question: Does the paper discuss the limitations of the work performed by the authors?

Answer: [Yes]

Justification: A detailed discussion of the limitations of this work is provided in Appendix L.

Guidelines:

- The answer NA means that the paper has no limitation while the answer No means that the paper has limitations, but those are not discussed in the paper.
- The authors are encouraged to create a separate "Limitations" section in their paper.
- The paper should point out any strong assumptions and how robust the results are to violations of these assumptions (e.g., independence assumptions, noiseless settings, model well-specification, asymptotic approximations only holding locally). The authors should reflect on how these assumptions might be violated in practice and what the implications would be.
- The authors should reflect on the scope of the claims made, e.g., if the approach was only tested on a few datasets or with a few runs. In general, empirical results often depend on implicit assumptions, which should be articulated.
- The authors should reflect on the factors that influence the performance of the approach. For example, a facial recognition algorithm may perform poorly when image resolution is low or images are taken in low lighting. Or a speech-to-text system might not be used reliably to provide closed captions for online lectures because it fails to handle technical jargon.
- The authors should discuss the computational efficiency of the proposed algorithms and how they scale with dataset size.
- If applicable, the authors should discuss possible limitations of their approach to address problems of privacy and fairness.
- While the authors might fear that complete honesty about limitations might be used by reviewers as grounds for rejection, a worse outcome might be that reviewers discover limitations that aren't acknowledged in the paper. The authors should use their best judgment and recognize that individual actions in favor of transparency play an important role in developing norms that preserve the integrity of the community. Reviewers will be specifically instructed to not penalize honesty concerning limitations.

3. Theory assumptions and proofs

Question: For each theoretical result, does the paper provide the full set of assumptions and a complete (and correct) proof?

Answer: [Yes]

Justification: Complete proofs for all newly introduced theorems are provided in the appendix, and all cited theorems are clearly attributed to their original sources.

Guidelines:

- The answer NA means that the paper does not include theoretical results.
- All the theorems, formulas, and proofs in the paper should be numbered and crossreferenced.
- All assumptions should be clearly stated or referenced in the statement of any theorems.
- The proofs can either appear in the main paper or the supplemental material, but if they appear in the supplemental material, the authors are encouraged to provide a short proof sketch to provide intuition.
- Inversely, any informal proof provided in the core of the paper should be complemented by formal proofs provided in appendix or supplemental material.
- Theorems and Lemmas that the proof relies upon should be properly referenced.

4. Experimental result reproducibility

Question: Does the paper fully disclose all the information needed to reproduce the main experimental results of the paper to the extent that it affects the main claims and/or conclusions of the paper (regardless of whether the code and data are provided or not)?

Answer: [Yes]

Justification: Pseudocode for the proposed method is provided in Algorithm 5 of the appendix, while Section C of the appendix includes all necessary experimental details to ensure reproducibility.

Guidelines:

- The answer NA means that the paper does not include experiments.
- If the paper includes experiments, a No answer to this question will not be perceived well by the reviewers: Making the paper reproducible is important, regardless of whether the code and data are provided or not.
- If the contribution is a dataset and/or model, the authors should describe the steps taken to make their results reproducible or verifiable.
- Depending on the contribution, reproducibility can be accomplished in various ways. For example, if the contribution is a novel architecture, describing the architecture fully might suffice, or if the contribution is a specific model and empirical evaluation, it may be necessary to either make it possible for others to replicate the model with the same dataset, or provide access to the model. In general, releasing code and data is often one good way to accomplish this, but reproducibility can also be provided via detailed instructions for how to replicate the results, access to a hosted model (e.g., in the case of a large language model), releasing of a model checkpoint, or other means that are appropriate to the research performed.
- While NeurIPS does not require releasing code, the conference does require all submissions to provide some reasonable avenue for reproducibility, which may depend on the nature of the contribution. For example
- (a) If the contribution is primarily a new algorithm, the paper should make it clear how to reproduce that algorithm.
- (b) If the contribution is primarily a new model architecture, the paper should describe the architecture clearly and fully.
- (c) If the contribution is a new model (e.g., a large language model), then there should either be a way to access this model for reproducing the results or a way to reproduce the model (e.g., with an open-source dataset or instructions for how to construct the dataset).
- (d) We recognize that reproducibility may be tricky in some cases, in which case authors are welcome to describe the particular way they provide for reproducibility. In the case of closed-source models, it may be that access to the model is limited in some way (e.g., to registered users), but it should be possible for other researchers to have some path to reproducing or verifying the results.

5. Open access to data and code

Question: Does the paper provide open access to the data and code, with sufficient instructions to faithfully reproduce the main experimental results, as described in supplemental material?

Answer: [Yes]

Justification: Source code is available at https://github.com/DOCU-Lab/Feedback-based_Conformal_Prediction.

Guidelines:

- The answer NA means that paper does not include experiments requiring code.
- Please see the NeurIPS code and data submission guidelines (https://nips.cc/public/guides/CodeSubmissionPolicy) for more details.
- While we encourage the release of code and data, we understand that this might not be
 possible, so "No" is an acceptable answer. Papers cannot be rejected simply for not
 including code, unless this is central to the contribution (e.g., for a new open-source
 benchmark).
- The instructions should contain the exact command and environment needed to run to reproduce the results. See the NeurIPS code and data submission guidelines (https://nips.cc/public/guides/CodeSubmissionPolicy) for more details.
- The authors should provide instructions on data access and preparation, including how
 to access the raw data, preprocessed data, intermediate data, and generated data, etc.
- The authors should provide scripts to reproduce all experimental results for the new proposed method and baselines. If only a subset of experiments are reproducible, they should state which ones are omitted from the script and why.
- At submission time, to preserve anonymity, the authors should release anonymized versions (if applicable).
- Providing as much information as possible in supplemental material (appended to the paper) is recommended, but including URLs to data and code is permitted.

6. Experimental setting/details

Question: Does the paper specify all the training and test details (e.g., data splits, hyperparameters, how they were chosen, type of optimizer, etc.) necessary to understand the results?

Answer: [Yes]

Justification: The experimental setting is provided in Section 6 of the main text and details are provided in Section C of the appendix.

Guidelines:

- The answer NA means that the paper does not include experiments.
- The experimental setting should be presented in the core of the paper to a level of detail that is necessary to appreciate the results and make sense of them.
- The full details can be provided either with the code, in appendix, or as supplemental
 material.

7. Experiment statistical significance

Question: Does the paper report error bars suitably and correctly defined or other appropriate information about the statistical significance of the experiments?

Answer: [Yes]

Justification: The standard deviations and coefficients of variation from multiple randomized experiments are reported in Section J of the appendix.

Guidelines:

- The answer NA means that the paper does not include experiments.
- The authors should answer "Yes" if the results are accompanied by error bars, confidence intervals, or statistical significance tests, at least for the experiments that support the main claims of the paper.

- The factors of variability that the error bars are capturing should be clearly stated (for example, train/test split, initialization, random drawing of some parameter, or overall run with given experimental conditions).
- The method for calculating the error bars should be explained (closed form formula, call to a library function, bootstrap, etc.)
- The assumptions made should be given (e.g., Normally distributed errors).
- It should be clear whether the error bar is the standard deviation or the standard error
 of the mean.
- It is OK to report 1-sigma error bars, but one should state it. The authors should preferably report a 2-sigma error bar than state that they have a 96% CI, if the hypothesis of Normality of errors is not verified.
- For asymmetric distributions, the authors should be careful not to show in tables or figures symmetric error bars that would yield results that are out of range (e.g. negative error rates).
- If error bars are reported in tables or plots, The authors should explain in the text how they were calculated and reference the corresponding figures or tables in the text.

8. Experiments compute resources

Question: For each experiment, does the paper provide sufficient information on the computer resources (type of compute workers, memory, time of execution) needed to reproduce the experiments?

Answer: [Yes]

Justification: The CPU model and RAM size are described in Section 6 of the main text, while the computational time for the experiments is included in the results table of each experiment. No additional computational effort beyond the reported experiments was required for the entire research project.

Guidelines:

- The answer NA means that the paper does not include experiments.
- The paper should indicate the type of compute workers CPU or GPU, internal cluster, or cloud provider, including relevant memory and storage.
- The paper should provide the amount of compute required for each of the individual experimental runs as well as estimate the total compute.
- The paper should disclose whether the full research project required more compute than the experiments reported in the paper (e.g., preliminary or failed experiments that didn't make it into the paper).

9. Code of ethics

Question: Does the research conducted in the paper conform, in every respect, with the NeurIPS Code of Ethics https://neurips.cc/public/EthicsGuidelines?

Answer: [Yes]

Justification: The research conducted in this paper adheres to the NeurIPS Code of Ethics in every respect.

Guidelines:

- The answer NA means that the authors have not reviewed the NeurIPS Code of Ethics.
- If the authors answer No, they should explain the special circumstances that require a deviation from the Code of Ethics.
- The authors should make sure to preserve anonymity (e.g., if there is a special consideration due to laws or regulations in their jurisdiction).

10. Broader impacts

Question: Does the paper discuss both potential positive societal impacts and negative societal impacts of the work performed?

Answer: [Yes]

Justification: A detailed discussion of the broader impacts is provided in Appendix M.

Guidelines:

- The answer NA means that there is no societal impact of the work performed.
- If the authors answer NA or No, they should explain why their work has no societal impact or why the paper does not address societal impact.
- Examples of negative societal impacts include potential malicious or unintended uses (e.g., disinformation, generating fake profiles, surveillance), fairness considerations (e.g., deployment of technologies that could make decisions that unfairly impact specific groups), privacy considerations, and security considerations.
- The conference expects that many papers will be foundational research and not tied to particular applications, let alone deployments. However, if there is a direct path to any negative applications, the authors should point it out. For example, it is legitimate to point out that an improvement in the quality of generative models could be used to generate deepfakes for disinformation. On the other hand, it is not needed to point out that a generic algorithm for optimizing neural networks could enable people to train models that generate Deepfakes faster.
- The authors should consider possible harms that could arise when the technology is being used as intended and functioning correctly, harms that could arise when the technology is being used as intended but gives incorrect results, and harms following from (intentional or unintentional) misuse of the technology.
- If there are negative societal impacts, the authors could also discuss possible mitigation strategies (e.g., gated release of models, providing defenses in addition to attacks, mechanisms for monitoring misuse, mechanisms to monitor how a system learns from feedback over time, improving the efficiency and accessibility of ML).

11. Safeguards

Question: Does the paper describe safeguards that have been put in place for responsible release of data or models that have a high risk for misuse (e.g., pretrained language models, image generators, or scraped datasets)?

Answer: [NA]

Justification: This paper poses no such risks.

Guidelines:

- The answer NA means that the paper poses no such risks.
- Released models that have a high risk for misuse or dual-use should be released with
 necessary safeguards to allow for controlled use of the model, for example by requiring
 that users adhere to usage guidelines or restrictions to access the model or implementing
 safety filters.
- Datasets that have been scraped from the Internet could pose safety risks. The authors should describe how they avoided releasing unsafe images.
- We recognize that providing effective safeguards is challenging, and many papers do
 not require this, but we encourage authors to take this into account and make a best
 faith effort.

12. Licenses for existing assets

Question: Are the creators or original owners of assets (e.g., code, data, models), used in the paper, properly credited and are the license and terms of use explicitly mentioned and properly respected?

Answer: [Yes]

Justification: This paper makes use of the TrajNet++ code, which was originally released by VITA Lab at EPFL. This code is publicly available at https://github.com/vita-epfl/trajnetplusplusbaselines and is licensed under the MIT License.

Guidelines:

- The answer NA means that the paper does not use existing assets.
- The authors should cite the original paper that produced the code package or dataset.
- The authors should state which version of the asset is used and, if possible, include a URL.

- The name of the license (e.g., CC-BY 4.0) should be included for each asset.
- For scraped data from a particular source (e.g., website), the copyright and terms of service of that source should be provided.
- If assets are released, the license, copyright information, and terms of use in the package should be provided. For popular datasets, paperswithcode.com/datasets has curated licenses for some datasets. Their licensing guide can help determine the license of a dataset.
- For existing datasets that are re-packaged, both the original license and the license of the derived asset (if it has changed) should be provided.
- If this information is not available online, the authors are encouraged to reach out to the asset's creators.

13. New assets

Question: Are new assets introduced in the paper well documented and is the documentation provided alongside the assets?

Answer: [NA]

Justification: This paper does not release new assets.

Guidelines:

- The answer NA means that the paper does not release new assets.
- Researchers should communicate the details of the dataset/code/model as part of their submissions via structured templates. This includes details about training, license, limitations, etc.
- The paper should discuss whether and how consent was obtained from people whose asset is used.
- At submission time, remember to anonymize your assets (if applicable). You can either create an anonymized URL or include an anonymized zip file.

14. Crowdsourcing and research with human subjects

Question: For crowdsourcing experiments and research with human subjects, does the paper include the full text of instructions given to participants and screenshots, if applicable, as well as details about compensation (if any)?

Answer: [NA]

Justification: This paper does not involve crowdsourcing nor research with human subjects. Guidelines:

- The answer NA means that the paper does not involve crowdsourcing nor research with human subjects.
- Including this information in the supplemental material is fine, but if the main contribution of the paper involves human subjects, then as much detail as possible should be included in the main paper.
- According to the NeurIPS Code of Ethics, workers involved in data collection, curation, or other labor should be paid at least the minimum wage in the country of the data collector.

15. Institutional review board (IRB) approvals or equivalent for research with human subjects

Question: Does the paper describe potential risks incurred by study participants, whether such risks were disclosed to the subjects, and whether Institutional Review Board (IRB) approvals (or an equivalent approval/review based on the requirements of your country or institution) were obtained?

Answer: [NA]

Justification: This paper does not involve crowdsourcing nor research with human subjects. Guidelines:

 The answer NA means that the paper does not involve crowdsourcing nor research with human subjects.

- Depending on the country in which research is conducted, IRB approval (or equivalent) may be required for any human subjects research. If you obtained IRB approval, you should clearly state this in the paper.
- We recognize that the procedures for this may vary significantly between institutions and locations, and we expect authors to adhere to the NeurIPS Code of Ethics and the guidelines for their institution.
- For initial submissions, do not include any information that would break anonymity (if applicable), such as the institution conducting the review.

16. Declaration of LLM usage

Question: Does the paper describe the usage of LLMs if it is an important, original, or non-standard component of the core methods in this research? Note that if the LLM is used only for writing, editing, or formatting purposes and does not impact the core methodology, scientific rigorousness, or originality of the research, declaration is not required.

Answer: [NA]

Justification: The core method development in this research does not involve LLMs as any important, original, or non-standard components.

Guidelines:

- The answer NA means that the core method development in this research does not involve LLMs as any important, original, or non-standard components.
- Please refer to our LLM policy (https://neurips.cc/Conferences/2025/LLM) for what should or should not be described.

A Auxiliary Results

A.1 Conformal Prediction Lemma

Lemma A.1 [Lemma 1 in Tibshirani et al. [2019]] (coverage guarantee) If $R^{(0)}, R^{(1)}, ..., R^{(N)}$ are N+1 exchangeable random variables, then for a failure probability $\alpha \in (0,1)$, it holds that

$$\mathbb{P}\left\{R^{(0)} \le Quantile_{1-\alpha}(R^{(1)}, ..., R^{(N)}, \infty)\right\} \ge 1 - \alpha \tag{19}$$

where the function $Quantile_{1-\alpha}(R^{(1)},...,R^{(N)},\infty)$ denotes the level $1-\alpha$ quantile of the empirical distribution of the values $R^{(1)},...,R^{(N)},\infty$ as follows.

$$Quantile_{1-\alpha}(R^{(1)}, ..., R^{(N)}, \infty) = \inf\{z : \mathbb{P}\{Z \le z\} \ge 1 - \alpha\},\tag{20a}$$

$$Z \sim \left(\sum_{i=1}^{N} \delta_{R^{(i)}} + \delta_{\infty}\right) / (N+1)$$
 (20b)

where $\delta_{R^{(i)}}$ and δ_{∞} denote the Dirac delta function at $R^{(i)}$ and ∞ , respectively.

A.2 Upper bound of the expectation of posterior risk

Corollary A.2 (upper bound of β_{τ}) Suppose that $\delta \in (0,1)$ and $K > (-\ln \delta)/(2\alpha_{\tau}^2)$, we have

$$\mathbb{P}\left\{\mathbb{E}(\beta_{\tau}) \le \left(1 + L\left(\alpha_{\tau} + \sqrt{-\ln\delta/(2K)}\right)\right) / (1 + L)\right\} \ge 1 - \delta \tag{21}$$

Furthermore if $K, L \to \infty$, then $\mathbb{E}(\beta_{\tau}) \le \alpha_{\tau}$ holds with probability one.

Remark A.3 Corollary A.2 provides a performance guarantee for Fb-CP, i.e. Fb-CP performs at least as well as the sequential method Lindemann et al. [2023] with high probability. Furthermore, the experiments in Section 6 demonstrate that the proposed method performs significantly better in practice. This is attributed to the conservatism of the inequality (38) in the proof of Corollary A.2. Since $c(x_{\tau}^*, Y_{\tau})$ contains the information provided by $c(\cdot)$ (e.g. the shape of the robot and obstacles) and x_{τ}^* , it typically occurs that $\mathbb{P}\{c(x_{\tau}^*, Y_{\tau}) < 0\} \ll \mathbb{P}\{\|Y_{\tau} - \hat{Y}_{\tau|t}\| > C_{\tau|t}^{1-\alpha_{\tau}}\}$.

B Proofs

B.1 Proof of Lemma 4.1

According to Assumptions 3.1 as well as the calculation of $C_{\tau|t}^{1-\alpha_{\tau}}$ (6b), the $(1-\alpha_{\tau})$ -coverage guarantee of the prediction (6a) is obtained through Lemma A.1. Note that the function c is L-Lipschitz continuous, the following inequality is obtained.

$$||c(x_{\tau}, Y_{\tau}) - c(x_{\tau}, \hat{Y}_{\tau|t})|| \le L||Y_{\tau} - \hat{Y}_{\tau|t}|| \Longrightarrow c(x_{\tau}, Y_{\tau}) \ge c(x_{\tau}, \hat{Y}_{\tau|t}) - L||Y_{\tau} - \hat{Y}_{\tau|t}||$$
 (22)

If the constraint $c(x_{\tau}, \hat{Y}_{\tau|t}) \geq LC_{\tau|t}^{1-\alpha_{\tau}}$ is satisfied, we have the following inequality.

$$c(x_{\tau}, Y_{\tau}) \ge L(C_{\tau|t}^{1-\alpha} - ||Y_{\tau} - \hat{Y}_{\tau|t}||)$$
(23)

According to the $(1 - \alpha_{\tau})$ -coverage guarantee (6a) $\mathbb{P}\{C_{\tau|t}^{1-\alpha} - \|Y_{\tau} - \hat{Y}_{\tau|t}\| \ge 0\} \ge 1 - \alpha_{\tau}$, the lemma is proven.

B.2 Proof of Lemma 4.2

According to Assumption 3.1, we know that all trajectories $Y^{(i)}$ are generated by sampling their initial state $Y_0^{(i)}$ from the same distribution $\mathbb D$ and then evolving using a common dynamics (the ground truth dynamics). As a result, the random variables $\omega_{\tau}, \omega_{\tau}^{(1)}, ..., \omega_{\tau}^{(K+L)}$ are i.i.d.. Note that x_{τ}^* is the true state of the system at time τ , thus x_{τ}^* is fixed and independent of $\omega_{\tau}, \omega_{\tau}^{(K+1)}, ..., \omega_{\tau}^{(K+L)}$. Therefore, the random variables $S_{\tau}, S_{\tau}^{(K+1)}, ..., S_{\tau}^{(K+L)}$ are exchangeable.

Without loss of generality, we assume that the dataset $\{-S_{\tau}^{(K+i)}: i=1,...,L\}$ are sorted in non-decreasing order. We first assume that $-S_{\tau}^{(K+1)} \leq 0$, and then we define the maximum index ℓ that makes $-S_{\tau}^{(K+\ell)} \leq 0$ hold as follows.

$$\ell = \max_{l=1,\dots,L} \quad l$$

$$s.t. \quad -S_{\tau}^{(K+\ell)} \le 0$$
(24)

Then the posterior satisfaction probability can be computed below.

$$\mathbb{P}\{c(x_{\tau}^*, Y_{\tau}) \ge 0\} = \mathbb{P}\{-S_{\tau} \le 0\} \ge \mathbb{P}\{-S_{\tau} \le -S_{\tau}^{(K+\ell)}\}$$
 (25)

It is assumed that there are t terms in $\{-S_{\tau}^{(K+i)}: i=1,...,L\}$ identical to $-S_{\tau}^{(K+\ell)}$, i.e.

$$-S_{\tau}^{(K+\ell-t)} < -S_{\tau}^{(K+\ell-t+1)} = \dots = -S_{\tau}^{(K+\ell)} \le 0 < -S_{\tau}^{(K+\ell+1)}$$
 (26)

Then $-S_{\tau}^{(K+\ell)}$ can be equivalently reformulated as follows.

$$-S_{\tau}^{(K+\ell)} = Quantile_{\beta}(-S_{\tau}^{(K+1)}, ..., -S_{\tau}^{(K+L)}, \infty), \quad \forall \beta \in \left(\frac{\ell-t}{1+L}, \frac{\ell}{1+L}\right]$$
 (27)

Combining (25) and (27) we have

$$\mathbb{P}\{c(x_{\tau}^*, Y_{\tau}) \ge 0\} \ge \mathbb{P}\{-S_{\tau} \le Quantile_{\beta}(-S_{\tau}^{(K+1)}, ..., -S_{\tau}^{(K+L)}, \infty)\}$$
(28)

Note that the random variables $S_{\tau}, S_{\tau}^{(K+1)}, ..., S_{\tau}^{(K+L)}$ are exchangeable and $\beta \in \left(\frac{\ell-t}{1+L}, \frac{\ell}{1+L}\right] \subset (0,1)$, and thus we can apply Lemma A.1 and obtain

$$\mathbb{P}\{c(x_{\tau}^*, Y_{\tau}) \ge 0\} \ge \beta, \quad \forall \beta \in \left(\frac{\ell - t}{1 + L}, \frac{\ell}{1 + L}\right)$$
(29)

Therefore, the upper bound of the posterior violation probability can be computed by

$$\mathbb{P}\{c(x_{\tau}^*, Y_{\tau}) < 0\} \le 1 - \beta, \quad \forall \beta \in \left(\frac{\ell - t}{1 + L}, \frac{\ell}{1 + L}\right)$$
(30)

To minimize this upper bound, we take the maximum value of β and (30) becomes (31).

$$\mathbb{P}\{c(x_{\tau}^*, Y_{\tau}) < 0\} \le 1 - \frac{\ell}{1 + L} \tag{31}$$

According to the definition of ℓ (24), we can compute ℓ as follows.

$$\ell = \sum_{i=1}^{L} \mathbb{I}\left(S_{\tau}^{(K+i)} \ge 0\right) = L - \sum_{i=1}^{L} \mathbb{I}\left(S_{\tau}^{(K+i)} < 0\right)$$
(32)

Combining (31) and (32), we have

$$\mathbb{P}\{c(x_{\tau}^*, Y_{\tau}) < 0\} \le \frac{1 + \sum_{i=1}^{L} \mathbb{I}\left(S_{\tau}^{(K+i)} < 0\right)}{1 + L}$$
(33)

Finally, we consider the scenario in which $-S_{\tau}^{(K+1)} > 0$, which means $S_{\tau}^{(K+i)} < 0 \ \forall i = 1, ..., L$. Then the inequality (33) is simplified as follows.

$$\mathbb{P}\{c(x_{\tau}^*, Y_{\tau}) < 0\} \le 1 \tag{34}$$

which is always true. Thus, the Lemma is proven.

B.3 Proof of Corollary A.2

Taking expectations on both sides of Equation (8), we can obtain

$$\mathbb{E}(\beta_{\tau}) = \frac{1 + L\mathbb{P}\{S_{\tau}^{(K+i)} < 0\}}{1 + L} = \frac{1 + L\mathbb{P}\{S_{\tau} < 0\}}{1 + L} = \frac{1 + L\mathbb{P}\{c(x_{\tau}^*, Y_{\tau}) < 0\}}{1 + L}$$
(35)

The second equality holds because $S_{\tau}, S_{\tau}^{K+1}, ..., S_{\tau}^{K+L}$ are exchangeable. Note that the function $c(\dot)$ is L-Lipschitz continuous and x_{τ}^* is a feasible solution of problem (3) with the reformulated constraint through Lemma 4.1, and the following inequality can be derived in the same manner as inequalities (22) and (23) in the Proof of Lemma 4.1 (Appendix B.1).

$$c(x_{\tau}^*, Y_{\tau}) \ge L(C_{\tau|t}^{1-\alpha_{\tau}} - \|Y_{\tau} - \hat{Y}_{\tau|t}\|)$$
(36)

Based on (36), we can obtain

$$c(x_{\tau}^*, Y_{\tau}) < 0 \Rightarrow ||Y_{\tau} - \hat{Y}_{\tau|t}|| > C_{\tau|t}^{1-\alpha_{\tau}}$$
 (37)

And the following inequality is derived.

$$\mathbb{P}\{c(x_{\tau}^*, Y_{\tau}) < 0\} \le \mathbb{P}\{\|Y_{\tau} - \hat{Y}_{\tau|t}\| > C_{\tau|t}^{1-\alpha_{\tau}}\}$$
(38)

Combining (35) and (38), we have

$$\mathbb{E}(\beta_{\tau}) \le \frac{1 + L\mathbb{P}\{\|Y_{\tau} - \hat{Y}_{\tau|t}\| > C_{\tau|t}^{1 - \alpha_{\tau}}\}}{1 + L}$$
(39)

For $\alpha_{\tau}, \delta \in (0,1)$ and $K > (-\ln \delta)/(2\alpha_{\tau}^2)$, we can apply [Vovk [2012], Proposition 2a] so that

$$\mathbb{P}\left\{\mathbb{P}\left\{\|Y_{\tau} - \hat{Y}_{\tau|t}\| \le C_{\tau|t}^{1-\alpha_{\tau}}\right\} \ge 1 - \left(\alpha_{\tau} + \sqrt{-\ln\delta/(2K)}\right)\right\} \ge 1 - \delta \tag{40}$$

which can be equivalently transformed into the following expression.

$$\mathbb{P}\left\{\mathbb{P}\left\{\|Y_{\tau} - \hat{Y}_{\tau|t}\| > C_{\tau|t}^{1-\alpha_{\tau}}\right\} \le \alpha_{\tau} + \sqrt{-\ln \delta/(2K)}\right\} \ge 1 - \delta \tag{41}$$

Combining (39) and (41), we can finally obtain the inequality (21).

When $K, L \to \infty$, we can further assume that $L \ge 1/\delta$ and $K \ge \max\{(-\ln \delta)/(2\alpha_\tau^2), 1/\delta\}$. Note that for a fixed α_τ , we can always find a small enough positive δ such that $\alpha_\tau + \sqrt{(-\ln \delta)/(2K)} < \alpha_\tau + \sqrt{(-\delta \ln \delta)/2} < 1$. Therefore for a small enough positive δ we have

$$\mathbb{P}\left\{\mathbb{E}(\beta_{\tau}) \leq \frac{\delta + \alpha_{\tau} + \sqrt{-\delta \ln \delta/2}}{\delta + 1}\right\}$$

$$\geq \mathbb{P}\left\{\mathbb{E}(\beta_{\tau}) \leq \frac{1 + L\left(\alpha_{\tau} + \sqrt{-\ln \delta/(2K)}\right)}{1 + L}\right\} \geq 1 - \delta$$
(42)

Let $\delta \to 0^+$, we finally obtain that $\mathbb{E}(\beta_{\tau}) \leq \alpha_{\tau}$ holds with probability one.

B.4 Proof of Lemma 5.1

Let $\alpha^1_{t+1:T}$ and $\alpha^2_{t+1:T}$ be two risk allocations at time t. Based on the definition of $C^{1-\alpha_{\tau}}_{\tau|t}$ (6b), $C^{1-\alpha_{\tau}}_{\tau|t}$ is non-increasing with respect to α_{τ} for fixed D^1_{cal} . Therefore, if $\alpha^1_{\tau} \leq \alpha^2_{\tau}$, $\forall \tau = t+1,...,T$, then $C^{1-\alpha^1_{\tau}}_{\tau|t} \geq C^{1-\alpha^2_{\tau}}_{\tau|t}$ which further leads to $\mathcal{R}_t(\alpha^1_{t+1:T}) \subseteq \mathcal{R}_t(\alpha^2_{t+1:T})$. Since $J^*(\alpha_{t+1:T})$ is the minimum of the objective problem (10) with the feasible region $\mathcal{R}_t(\alpha_{t+1:T})$, $J^*(\alpha^1_{t+1:T}) \geq J^*(\alpha^2_{t+1:T})$ can be obtained and the lemma is proven.

B.5 Proof of Lemma 5.2

The computation of the lower bound is analogous to the calculation of β_{τ} in Lemma 4.1, except that Lemma A.1 is not required to obtain coverage guarantees. Therefore, the computation is based on D^1_{cal} . Without loss of generality, we assume that the dataset $\{R^{(i)}_{\tau|t}: i=1,...,K\}$ is sorted in non-decreasing order. Note that $x^n_{t+1:T}$ is feasible for the problem (10) with $\alpha^n_{t+1:T}$ and $\tau \in \mathcal{I}_{ina}$, the inequality $c(x^n_{\tau}, \hat{Y}_{\tau|t}) > LC^{1-\alpha^n_{\tau}}_{\tau|t} = LQuantile_{1-\alpha^n_{\tau}}(R^{(1)}_{\tau|t},...,R^{(K)}_{\tau|t},\infty)$ holds true. Since $\alpha^n_{\tau} < 1$, it follows that $c(x^n_{\tau}, \hat{Y}_{\tau|t}) > R^{(1)}_{\tau|t}$. Therefore, we define the maximum index \mathcal{K} that makes $c(x^n_{\tau}, \hat{Y}_{\tau|t}) \geq LR^{(\mathcal{K})}_{\tau|t}$ hold as follows.

$$\mathcal{K} = \max_{k=1,\dots,K} k$$

$$s.t. \quad c(x_{\tau}^{n}, \hat{Y}_{\tau|t}) \ge LR_{\tau|t}^{(k)}$$

$$(43)$$

It is assumed that there are t terms in $\{R_{\tau|t}^{(i)}: i=1,...,K\}$ identical to $R_{\tau|t}^{\mathcal{K}}$, and thus we can obtain

$$R_{\tau|t}^{(\mathcal{K}-t)} < R_{\tau|t}^{(\mathcal{K}-t+1)} = \dots = R_{\tau|t}^{(\mathcal{K})} \le c(x_{\tau}^n, \hat{Y}_{\tau|t})/L < R_{\tau|t}^{(\mathcal{K}+1)}$$
(44)

We aim to determine the maximum value of $C_{\tau|t}^{1-\widetilde{\alpha}_{\tau}^{n}}$ (the minimum value of $\widetilde{\alpha}_{\tau}^{n}$) while satisfying $C_{\tau|t}^{1-\widetilde{\alpha}_{\tau}^{n}} \leq c(x_{\tau}^{n},\hat{Y}_{\tau|t})/L$, which is equivalent to $C_{\tau|t}^{1-\widetilde{\alpha}_{\tau}^{n}} \leq R_{\tau|t}^{\mathcal{K}}$ because $C_{\tau|t}^{1-\widetilde{\alpha}_{\tau}^{n}}$ can only take values at a finite number of discrete points $R_{\tau|t}^{(1)},...,R_{\tau|t}^{(K)},\infty$. Furthermore, $R_{\tau|t}^{\mathcal{K}}$ can be equivalently reformulated as follows.

$$R_{\tau|t}^{\mathcal{K}} = Quantile_{\beta}(R_{\tau|t}^{(1)}, ..., R_{\tau|t}^{(K)}, \infty) = C_{\tau|t}^{\beta}, \quad \forall \beta \in \left(\frac{\mathcal{K} - t}{1 + K}, \frac{\mathcal{K}}{1 + K}\right]$$
(45)

Therefore, the constraint $C_{\tau|t}^{1-\widetilde{\alpha}_{\tau}^n} \leq R_{\tau|t}^{\mathcal{K}}$ is equivalent to the following expression.

$$C_{\tau|t}^{1-\tilde{\alpha}_{\tau}^{n}} \le C_{\tau|t}^{\beta}, \quad \exists \beta \in \left(\frac{\mathcal{K}-t}{1+K}, \frac{\mathcal{K}}{1+K}\right]$$
(46)

Note that $C_{\tau|t}^{\beta}$ is non-decreasing with respect to β for fixed D_{cal}^{1} . Constraint (46) is further reformulated as follows.

$$\widetilde{\alpha}_{\tau}^{n} \ge 1 - \frac{\mathcal{K}}{1 + K} \tag{47}$$

According to the definition of K (43), we can compute K in (48).

$$\mathcal{K} = \sum_{i=1}^{K} \mathbb{I}\left(c(x_{\tau}^{n}, \hat{Y}_{\tau|t}) \ge LR_{\tau|t}^{(i)}\right) = K - \sum_{i=1}^{K} \mathbb{I}\left(c(x_{\tau}^{n}, \hat{Y}_{\tau|t}) < LR_{\tau|t}^{(i)}\right) \tag{48}$$

Combining (47) and (48), the lower bound of $\tilde{\alpha}_{\tau}^{n}$ is computed as follows.

$$\underline{\alpha}_{\tau}^{n} = \frac{1 + \sum_{i=1}^{K} \mathbb{I}\left(c(x_{\tau}^{n}, \hat{Y}_{\tau|t}) < LR_{\tau|t}^{(i)}\right)}{1 + K} \tag{49}$$

We note that $\underline{\alpha}_{\tau}^{n}$ is the lower bound of $\widetilde{\alpha}_{\tau}^{n}$ that ensures the constraint $c(x_{\tau}^{n}, \hat{Y}_{\tau|t}) \geq LC_{\tau|t}^{1-\widetilde{\alpha}_{\tau}^{n}}$. Furthermore, since $x_{t+1:T}^{n}$ is feasible for the problem (10) with $\alpha_{t+1:T}^{n}$, the constraint $c(x_{\tau}^{n}, \hat{Y}_{\tau|t}) \geq LC_{\tau|t}^{1-\alpha_{\tau}^{n}}$ is satisfied. Therefore, $\underline{\alpha}_{\tau}^{n} \leq \alpha_{\tau}^{n}$ is naturally obtained. Thus the Lemma is proven.

B.6 Proof of Theorem 5.3

The proof adapts elements of the proof from Zymler et al. [2013]. If $x_{t+1:T}^0$, $u_{t:T-1}^0$ is a feasible solution for the risk allocation $\alpha_{t+1:T}^0$, the update law of $\alpha_{t+1:T}$ guarantees that the sequence of the optimal objective values $\{J^*(\alpha_{t+1:T}^n)\}_{n\in\mathbb{N}}$ is monotonically decreasing, as previously mentioned. Since the sets \mathcal{X} and \mathcal{U} are bounded, $x_{t+1:T}$ and $u_{t:T-1}$ are bounded. Because the objective function $J(x_{t+1:T}, u_{t:T-1})$ is continuous, the boundedness of $x_{t+1:T}$, $x_{t:T-1}$ and the monotonicity of the optimal objective value sequence imply that $\{J^*(\alpha_{t+1:T}^n)\}_{n\in\mathbb{N}}$ converges to a finite limit.

B.7 Proof of Theorem 5.4

At each time t, the realized state $x_{1:t}^*$ is available. According to Lemma 4.2, we know that

$$\mathbb{P}\{c(x_{\tau}^*, Y_{\tau}) < 0\} \le \beta_{\tau}, \quad \forall \tau = 1, ..., t$$
 (50)

For the planned state $x_{t+1:T}^*$, the corresponding risk allocations $\alpha_{t+1:T}$ are obtained either via ARA (11) or IRA (12). In both cases, they satisfy

$$\sum_{\tau=t+1}^{T} \alpha_{\tau} \le \alpha - \sum_{\tau=1} \beta_{\tau} \tag{51}$$

We note that if the planned state $x_{t+1:T}^*$ is a feasible solution of the TO problem (10) with $\alpha_{t+1:T}$, the following inequality can be obtained through Lemma 4.1.

$$\mathbb{P}\{c(x_{\tau}^*, Y_{\tau}) \ge 0\} \ge 1 - \alpha_{\tau}, \quad \forall \tau = t + 1, ..., T$$
 (52)

Finally, by combining the above three inequalities (50), (51), and (52), together with Boole's inequality, we obtain

$$\mathbb{P}\{\bigcap_{\tau=1}^{T} \{C(x_{\tau}^*, Y_{\tau}) \ge 0\}\} \ge 1 - \alpha \tag{53}$$

which means that the overall risk of the entire trajectory at time $t, x_{1:T}^*$ is below the risk tolerance α . Thus, Theorem 5.4 is proven.

C Experiment details and additional results

C.1 Simulation for a kinematic vehicle model

We examine the kinematic vehicle model Lekeufack et al. [2024] with the following nonlinear dynamics.

$$\begin{bmatrix} p_{x,t+1} \\ p_{y,t+1} \\ \theta_{t+1} \\ v_{t+1} \end{bmatrix} = \begin{bmatrix} p_{x,t} + \Delta v_t \cos \theta_t \\ p_{y,t} + \Delta v_t \sin \theta_t \\ \theta_t + \Delta \frac{v_t}{l} \tan \phi_t \\ v_t + \Delta a_t \end{bmatrix}$$
(54)

where $p_t := (p_{x,t}, p_{y,t})$, θ_t , v_t are the position, orientation, and velocity of the vehicle, respectively. l := 0.2 is the length, and $\Delta = 0.125$ is the sampling time. The system inputs are the steering angle $\phi_t \in [-\pi/6, \pi/6]$ and the acceleration $a_t \in [-5, 5]$. The total time is set to T = 20. The objective is to reach the vicinity of the target point while avoiding collisions with obstacles. Formally, the objective function is defined as $J = \sum_{\tau=t}^{T-1} 100\phi_{\tau}^2 + a_{\tau}^2$ to minimize energy consumption and the constraint $\|p_T - p_{tar}\|_2 \le 0.2$ is incorporated into (9) to ensure the vehicle reaches the target point, where p_{tar} is the target point. The constraint function for collision avoidance is as follows.

$$c(p_{\tau}, Y_{\tau}) = \min_{j=1,\dots,M} \|p_{\tau}, Y_{\tau,j}\|_{2} - r_{r} - r_{o} - r_{s}$$
(55)

where r_r and r_o are the inflation radius of the vehicle and obstacle, respectively. r_s is the safety margin. The interior-point method-based solver IPOPT (v3.12.9) was used to solve the TO problem (9). Similar to Lindemann et al. [2023], we consider M=3 obstacles, with their trajectories generated by TrajNet++ Kothari et al. [2021] which is publicly available at https://github.com/vita-epfl/trajnetplusplusbaselines and is licensed under the MIT License. We generate 13,000 joint obstacle trajectories and randomly divide them into training D_{train} , calibration D_{cal} , and test D_{test} datasets with the set sizes 2,000, 10,000, and 1,000, respectively. We train an LSTM Alahi et al. [2016] using D_{train} as the trajectory predictor. For the proposed Fb-CP, D_{cal} is further divided into D_{cal}^1 and D_{cal}^2 with sizes $|D_{cal}^1|=2,000$ and $|D_{cal}^2|=8,000$. We conduct 1,000 Monte Carlo simulations using D_{test} . As we discussed in Section 6, the methods S-CP, Fb-CP-ARA, and Fb-CP-IRA are analyzed.

Table 2 shows the average cost, average computation time, and collision avoidance rate of 1,000 simulations using the kinematic vehicle model with different methods. We collect the simulation data under different total risk tolerances $\alpha = 0.05, 0.10, 0.15, 0.20$. On one hand, with an increase in

total risk tolerance, the average cost of all methods decreases. On the other hand, benefiting from the feedback information of posterior probabilities, the average cost of Fb-CP-ARA shows a reduction of 7.21% to 11.26% compared to S-CP. Furthermore, by flexibly allocating the allowable risk provided by posterior probabilities, the average cost of Fb-CP with IRA exhibits a significant reduction compared with S-CP. Additionally, the increase in total risk tolerance provides greater flexibility in the risk allocation of Fb-CP-IRA, resulting in a significant reduction in its average cost. As mentioned in Section 6, the calculation of posterior probabilities does not incur additional computational burden. Therefore, the average computation time of Fb-CP-ARA is essentially comparable to that of S-CP. The collision rates of all methods do not exceed their corresponding total risk tolerances.

Table 2: Average cost, computation time, and collision avoidance rate using the kinematic vehicle model with different methods.

| | | Sequential CP | Fb-C | CP |
|--------------------------|-----------------|---------------|----------|----------|
| | | Sequential Ci | with ARA | with IRA |
| | $\alpha = 0.05$ | 22.20 | 20.46 | 4.77 |
| Average cost | $\alpha = 0.10$ | 20.24 | 18.78 | 3.52 |
| Average cost | $\alpha = 0.15$ | 19.22 | 17.35 | 3.18 |
| | $\alpha = 0.20$ | 17.05 | 15.13 | 2.89 |
| | $\alpha = 0.05$ | 0.111 | 0.100 | 0.128 |
| Avamaga commutation time | $\alpha = 0.10$ | 0.093 | 0.087 | 0.126 |
| Average computation time | $\alpha = 0.15$ | 0.078 | 0.085 | 0.130 |
| | $\alpha = 0.20$ | 0.076 | 0.078 | 0.131 |
| | $\alpha = 0.05$ | 95.4% | 95.7% | 98.4% |
| Collision avoidance rate | $\alpha = 0.10$ | 93.9% | 93.1% | 98.3% |
| Collision avoidance rate | $\alpha = 0.15$ | 90.8% | 89.8% | 97.6% |
| | $\alpha = 0.20$ | 88.4% | 89.1% | 91.2% |

C.2 Simulation for linear quadrotor model

We examine the quadrotor model Dixit et al. [2023] with the following linear dynamics.

$$\ddot{x} = g\theta \qquad \ddot{y} = -g\phi \qquad \ddot{z} = \frac{1}{m_Q} u_1$$

$$\ddot{\phi} = \frac{l_Q}{I_{xx}} u_2 \qquad \ddot{\theta} = \frac{l_Q}{I_{yy}} u_3 \qquad \ddot{\psi} = \frac{l_Q}{I_{zz}} u_4$$
(56)

where g=9.81 represents the gravitational acceleration, $m_Q=0.65$ denotes the mass, and $l_Q=0.23$ is the distance between the quadrotor and the rotor. $I_{xx}=0.0075,\ I_{yy}=0.0075,$ and $I_{zz}=0.013$ correspond to the area moments of inertia about the principle axes in the body frame. The states are the position and orientation with the corresponding velocities and rates — $(x,y,z,\dot{x},\dot{y},\dot{z},\phi,\theta,\psi,\dot{\phi},\dot{\theta},\dot{\psi})\in\mathbb{R}^{12}$. The control inputs u_1,u_2,u_3,u_4 correspond to the thrust force in the body frame and three moments. The system (56) is discretized using the sampling time $\Delta=0.125$, and the total time is also set to T=20.

Similar to the experiments based on the kinematic vehicle model in Appendix C.1, the objective is to control the quadrotor to reach the target point p_{tar} while navigating around M=3 moving obstacles. The target point constraint and obstacle avoidance constraints are consistent with those used in the simulation using the kinematic vehicle model. We randomly generate 13,000 obstacle trajectories and assign them as in Appendix C.1. The following state-of-art methods recently proposed in the literature are analyzed through 1,000 Monte Carlo simulations.

- (i) Conformal Control (CC) proposed in Lekeufack et al. [2024].
- (ii) ACI for Motion Planning (ACI-MP) proposed in Dixit et al. [2023].
- (iii) Recursively Feasible MPC using CP (RF-CP) proposed in Stamouli et al. [2024]
- (iv) Sequential CP (S-CP) proposed in Lindemann et al. [2023]. Computation of the CP region and TO is performed sequentially.
- (v) Fb-CP with ARA (Fb-CP-ARA): The method based on Fb-CP using average risk allocation.
- (vi) Fb-CP with IRA (Fb-CP-IRA): The method based on Fb-CP using iterative risk allocation.

Table 3 shows the average cost, average computation time, and collision avoidance rate of 1,000 simulations using the quadrotor model with different methods. For the methods S-CP, Fb-CP-ARA,

Table 3: Average cost, computation time, and collision avoidance rate using the quadrotor model with different methods (η is the learning rate of CC).

| | | CC | | ACI-MP | RF-CP | S-CP | Fb-CP | |
|---------------------|---------------|-------|-----------------|--------|--------|--------|--------|-------|
| | | | | | | | ARA | IRA |
| | $\eta = 1000$ | 59.25 | $\alpha = 0.05$ | 17.970 | 15.794 | 17.321 | 15.356 | 7.189 |
| Average | $\eta = 500$ | 47.50 | $\alpha = 0.10$ | 17.263 | 14.378 | 16.17 | 14.228 | 6.798 |
| cost | $\eta = 100$ | 22.46 | $\alpha = 0.15$ | 16.096 | 11.922 | 14.83 | 12.354 | 6.191 |
| | $\eta = 50$ | 21.34 | $\alpha = 0.20$ | 15.310 | 10.032 | 13.217 | 10.22 | 5.398 |
| A | $\eta = 1000$ | 0.019 | $\alpha = 0.05$ | 0.022 | 0.487 | 0.022 | 0.027 | 0.038 |
| Average computation | $\eta = 500$ | 0.019 | $\alpha = 0.10$ | 0.026 | 0.494 | 0.020 | 0.021 | 0.039 |
| time | $\eta = 100$ | 0.021 | $\alpha = 0.15$ | 0.021 | 0.545 | 0.021 | 0.020 | 0.037 |
| time | $\eta = 50$ | 0.022 | $\alpha = 0.20$ | 0.022 | 0.500 | 0.020 | 0.019 | 0.036 |
| Collision | $\eta = 1000$ | 97.0% | $\alpha = 0.05$ | 98.6% | 98.7% | 98.8% | 98.2% | 96.3% |
| avoidance | $\eta = 500$ | 92.8% | $\alpha = 0.10$ | 93.3% | 96.9% | 93.5% | 94.6% | 94.1% |
| | $\eta = 100$ | 82.5% | $\alpha = 0.15$ | 91.5% | 92.4% | 92.0% | 90.2% | 91.9% |
| rate | $\eta = 50$ | 79.1% | $\alpha = 0.20$ | 87.9% | 90.0% | 88.2% | 86.7% | 88.2% |

and Fb-CP-IRA, the experimental results using the quadrotor model are fundamentally consistent with those derived from the experiments using the kinematic vehicle model. Specifically, compared with S-CP, Fb-CP-ARA benefits from the posterior probabilities calculation, leading to a moderate improvement in performance. Fb-CP-IRA, leveraging the combined use of posterior probabilities and a more flexible risk allocation, exhibits a significant enhancement in performance. Additionally, since CC and ACI-MP fail to fully utilize the information in the calibration dataset, they incur higher costs, which are 184% and 296% higher than those of Fb-CP-IRA, respectively. Particularly for CC, it directly controls the collision avoidance rate by adjusting the weight of the collision penalty term in the objective function, which results in a higher average cost. However, it should be noted that, in practice, CC and ACI-MP are better suited for scenarios where the test data exhibit distribution shift, rather than the setup considered in our work. For RF-CP, thanks to the proposed normalized nonconformity score, its average cost is comparable to that of Fb-CP-ARA, but it remains 85.8% higher than Fb-CP-IRA. However, the normalized nonconformity score introduces mixed-integer variables into the TO problem, significantly increasing the computation time. As shown in Table 3, the average computation time of RF-CP is more than an order of magnitude higher than that of Fb-CP-IRA.

C.3 Simulation for dynamic bicycle model

We examine a vehicle with the following dynamic bicycle model Hakobyan and Yang [2021].

$$\dot{x} = v_x \cos \theta - v_y \sin \theta \tag{57}$$

$$\dot{y} = v_x \sin \theta + v_y \cos \theta \tag{58}$$

$$\theta = r$$
 (59)

$$\dot{v_y} = \frac{-2(C_f + C_r)}{m_V v_x} v_y - \left(\frac{2l_f C_f - 2l_r C_r}{m_V v_x} + v_x\right) r + \frac{2C_f}{m_V} \delta_f \tag{60}$$

$$\dot{r} = \frac{-2(l_f C_f + l_r C_r)}{I_z v_x} v_y - \frac{2l_f^2 C_f - 2l_r^2 C_r}{I_z v_x} r + \frac{2l_f C_f}{I_z} \delta_f \tag{61}$$

where x,y are the vehicle's central of mass, θ,v_y , and r are lateral velocity, orientation, and yaw rate, respectively. Furthermore, v_x is the constant longitudinal velocity, m_V denotes the mass of the vehicle, C_f and C_r represent the cornering stiffness coefficients of the front and rear tires respectively, L_f and L_r denote the distances from the center of mass to the front and rear wheels, and I_z corresponds to the moment of inertia around the z-axis. The input variable is the front wheel steering angle δ_f . The system (57) is discretized using the sampling time $\Delta=0.125$, and the total time is also set to T=20. According to Hakobyan and Yang [2021], the parameters of the dynamic bicycle model used in this simulation are listed in Table 4.

Table 4: Dynamic bicycle model parameters.

| m_V | C_f | C_r | I_z | L_f | L_r | v_x |
|---------------------|----------|----------|--------------------|-------|-------|-------|
| $\overline{1700kg}$ | 50kN/rad | 50kN/rad | $6000kg \cdot m^2$ | 1.2m | 1.3m | 5m/s |

The task is to steer the vehicle to its target point p while avoiding M=2 moving obstacles. Similar to the experiments in Appendix C.1, the target point constraint and obstacle avoidance constraints are incorporated into the optimization problem to ensure the vehicle reaches the target point while avoiding collisions with obstacles. We collect 13,000 joint obstacle trajectories and assign them as in Appendix C.1. The methods S-CP, Fb-CP-ARA, and Fb-CP-IRA are analyzed through 1,000 Monte Carlo simulations.

Table 5 shows the average cost, average computation time, and collision avoidance rate of 1,000 simulations using the dynamic bicycle model with different methods. The experimental results are generally consistent with those obtained from the experiments using the kinematic vehicle mode and the quadrotor model. The performance of Fb-CP shows a certain degree of improvement over S-CP based on posterior probability calculations. Based on posterior probability calculations, Fb-CP-ARA demonstrates a certain level of performance improvement compared to S-CP, while Fb-CP-IRA further attains significant performance by leveraging the combined use of posterior probabilities and a more flexible risk allocation. It should be noted that, due to the simulation of a relatively complex nonlinear model in this experiment, the average computation time inevitably increases. Furthermore, it may be observed that the reduction in average cost achieved by Fb-CP-IRA compared to S-CP decreases in this experiment (47.2% reduction) compared with the experiment using the kinematic vehicle model in Appendix C.1 (81.9% reduction). This is because, compared to relatively simple scenarios (2 obstacles, dynamic bicycle model experiment), more complex scenarios (3 obstacles, kinematic vehicle model experiment) better highlight the performance improvements enabled by the flexibility in risk allocation.

Table 5: Average cost, computation time, and collision avoidance rate using the dynamic bicycle model with different methods.

| | | S-CP | Fb- | CP |
|--------------------------|-----------------|-------|-------|-------|
| | | 5 61 | ARA | IRA |
| | $\alpha = 0.05$ | 23.05 | 20.91 | 13.77 |
| A | $\alpha = 0.10$ | 22.38 | 18.39 | 11.35 |
| Average cost | $\alpha = 0.15$ | 20.71 | 16.99 | 10.17 |
| | $\alpha = 0.20$ | 16.55 | 14.78 | 8.58 |
| | $\alpha = 0.05$ | 0.365 | 0.361 | 0.884 |
| Avaraga computation time | $\alpha = 0.10$ | 0.339 | 0.335 | 0.817 |
| Average computation time | $\alpha = 0.15$ | 0.494 | 0.506 | 1.292 |
| | $\alpha = 0.20$ | 0.309 | 0.407 | 1.003 |
| | $\alpha = 0.05$ | 96.8% | 96.5% | 97.0% |
| Collision avoidance rate | $\alpha = 0.10$ | 94.8% | 94.0% | 94.3% |
| Comsion avoidance rate | $\alpha = 0.15$ | 91.5% | 90.0% | 91.5% |
| | $\alpha = 0.20$ | 89.5% | 87.8% | 89.5% |

In summary, the three simulation experiments demonstrate the general applicability of the proposed method, achieving significant performance improvements across various system models while satisfying probabilistic collision avoidance requirements. In fact, the complexity of different system models only affects the average computation time. In addition, simulations demonstrate that Fb-CP-IRA achieves more significant performance improvements in relatively complex scenarios.

C.4 Stanford Drone Dataset

We perform a comparative evaluation of different methods on the Stanford Drone Dataset. Specifically, the task is to steer the vehicle to its target point while avoiding moving obstacles (humans). Similar to the experiments in Appendix C.1, the target point constraint and obstacle avoidance constraints

are incorporated into the optimization problem to ensure the vehicle reaches the target point while avoiding collisions with obstacles. The average cost of different methods are summarized in Table 6.

As shown in Table 6, compared with S-CP, Fb-CP-ARA benefits from the posterior probabilities calculation, resulting in an average cost reduction of at least 20.7%. Fb-CP-IRA reduces the cost by at least 46% compared to S-CP. Additionally, since CC and ACI-MP fail to fully utilize the information in the calibration dataset, they incur higher costs, which are 176% and 113% higher than those of Fb-CP-IRA, respectively. Note that RF-CP is not included as a baseline because its formulation introduces mixed-integer variables through nonconformity score definitions, which—when combined with the nonlinear vehicle dynamics—leads to highly complex trajectory optimization problems with prohibitively long computation times.

Table 6: Average cost of different methods on the Real-World Stanford Drone Dataset with different methods.

| | | CC | | ACI-MP | S-CP | Fb- | -CP |
|---------|---------------|-------|-----------------|-----------|-------|-------|-------|
| | | | | 1101 1111 | 2 01 | ARA | IRA |
| | $\eta = 1000$ | 95.51 | $\alpha = 0.05$ | 40.02 | 38.58 | 30.58 | 20.81 |
| Average | $\eta = 500$ | 77.68 | $\alpha = 0.10$ | 35.94 | 34.75 | 27.52 | 18.52 |
| cost | $\eta = 100$ | 41.27 | $\alpha = 0.15$ | 32.57 | 30.48 | 23.75 | 15.58 |
| | $\eta = 50$ | 38.73 | $\alpha = 0.20$ | 29.89 | 28.59 | 21.25 | 14.02 |

D Experiment with different trajectory predictor

As noted in Subsection 3.1, employing the more advanced trajectory predictors can enhance control performance. Accordingly, we perform experiments on the kinematic vehicle model (54) to compare the average costs of S-CP and Fb-CP when using different predictors Social LSTM Alahi et al. [2016], Trajectron++ Salzmann et al. [2020], AgentFormer Yuan et al. [2021], with the results summarized in Table 7. As shown in Table 7, when switching to more advanced predictors Trajectron++ and AgentFormer, both Fb-CP and S-CP see improved performance, but the proposed method (Fb-CP) continues to outperform the S-CP under all tested predictors.

Table 7: Average Cost of Different Methods using Different Trajectory Predictors ($\alpha = 0.2$).

| | S-CP | Fb-CP-ARA | Fb-CP-IRA |
|--------------|-------|-----------|-----------|
| Social LSTM | 17.30 | 15.49 | 2.97 |
| Trajectron++ | 13.58 | 10.58 | 1.81 |
| AgentFormer | 12.83 | 9.71 | 1.72 |

E Experiment with small calibration size

As discussed in the Limitation (Appendix L), the proposed method requires a larger calibration dataset because the calibration dataset must be divided into two parts. To rigorously evaluate its performance under data-scarce conditions, we conduct experiments on the kinematic vehicle model (54), where both S-CP and Fb-CP are tested using the same small calibration dataset (N=400). The corresponding average costs, computation time, and collision avoidance rate are reported in Table 8. As shown in Table 8, although all methods see a decrease in performance under limited data, Fb-CP still achieves substantially lower cost than S-CP and remains safety. This highlights the robustness and practical effectiveness of the proposed method, even when the calibration dataset is small.

F Experiment with higher-dimensional settings

In this appendix, we validate the performance of the proposed method in high-dimensional settings. Specifically, we conduct an additional case study on controlling the trajectory of a high-dimensional

Table 8: Average Cost, computation time, and collision avoidance rate of Different methods with calibration data size of N=400.

| | S-CP | Fb-CP-ARA | Fb-CP-IRA |
|--------------------------|-------|-----------|-----------|
| Average cost | 18.03 | 16.82 | 3.52 |
| Average computation time | 0.078 | 0.081 | 0.122 |
| Collision avoidance rate | 88.9% | 89.5% | 91.7% |

double integrator model, where shrinking-horizon trajectory optimization is performed in 5- and 10-dimensional spaces. The average costs and collision probabilities of different methods under various dimensions are summarized in Table 9. As shown in Table 9, the proposed Fb-CP framework consistently outperforms S-CP while maintaining safety, even in these higher-dimensional scenarios. These results validate the applicability and effectiveness of the proposed approach in high-dimensional problems.

Table 9: Average cost and collision avoidance rate of different methods ($\alpha=0.2$) with varying dimensions.

| | Dimension | S-CP | Fb-CP-ARA | Fb-CP-IRA |
|--------------------------|-----------|-------|-----------|-----------|
| Average cost | 5 | 44.52 | 39.67 | 30.25 |
| | 10 | 72.66 | 65.33 | 60.18 |
| Collision avoidance rate | 5 | 92.5% | 92.1% | 93.5% |
| Comsion avoidance rate | 10 | 91.2% | 93.5% | 91.4% |

G Extension and experiments on distribution shift

The individual chance constraint reformulation in Lemma 4.1 and the posterior probability calculation in Lemma 4.2 rely on Assumption 3.1 and the i.i.d. property of ω , which imply that real joint obstacle trajectory and those in the training and calibration datasets follow the same distribution. To enhance the generalizability of the proposed method across different scenarios, we extend our method to address the case where a shift exists between the initial state distributions of calibration data and test data, and the error ω_t represents state-dependent noise rather than being i.i.d.

Specifically, there exists a shift between the initial obstacle state distribution \mathcal{D}_{test} of the test data and the initial obstacle state distribution \mathcal{D}_{cal} of the calibration data. Moreover, the error ω_t constitutes state-dependent noise, i.e., its distribution \mathcal{D}_{ω_t} is conditioned on the current state Y_t . Clearly, the difference between \mathcal{D}_{test} and \mathcal{D}_{cal} , along with the state-dependent nature of ω_t , implies that the test trajectories Y_t and the calibration trajectories $Y_t^{(i)}$ are not exchangeable. Fortunately, the distribution shift between Y_t and $Y_t^{(i)}$ can be characterized as a covariate shift, as defined in Tibshirani et al. [2019]. This allows us to adapt the approach proposed in Tibshirani et al. [2019] to extend our method accordingly. The extended method is described in detail below.

Intuitively, we reweight the calibration data by computing the likelihood ratio between the test and calibration distributions. The reweighted data are then used to compute the prediction regions and the posterior probabilities, thereby enabling robustness to covariate shift. Specifically, at each time t, we begin by applying an uncertainty propagation technique to derive the distributions $\widetilde{\mathcal{D}}_{Y_t}$ and \mathcal{D}_{Y_t} of the test obstacle state Y_t and calibration obstacle state $Y_t^{(i)}$, respectively. As a result, given a data Y, we can calculate the likelihood ratio as follows.

$$v(Y) = d\mathbb{P}_{\widetilde{\mathcal{D}}_{Y_t}}(Y)/d\mathbb{P}_{\mathcal{D}_{Y_t}}(Y)$$
(62)

In the forward phase of confidence region computation, the weights for the test data and the calibration data in D^1_{cal} are computed using the likelihood ratios (62) as follows.

$$p_1(Y_t) = \frac{v(Y_t)}{\sum_{j=1}^K v(Y_t^{(j)}) + v(Y_t)}, \quad p_1(Y_t^{(i)}) = \frac{v(Y_t^{(i)})}{\sum_{j=1}^K v(Y_t^{(j)}) + v(Y_t)}, \quad \forall i = 1, ..., K \quad (63)$$

Following the approach in Tibshirani et al. [2019], we replace the $(1 - \alpha)$ -quantile in equation 6b with the following weighted form.

$$C_{\tau|t}^{1-\alpha_{\tau}} = Quantile_{1-\alpha_{\tau}} \left(\sum_{i=1}^{K} p_1(Y_t^i) \delta_{R_{\tau|t}^{(i)}} + p_1(Y_t) \delta_{\infty} \right)$$
 (64)

In the process of backward posterior probability computation, we calculate the weights for the test data and the calibration data in D_{cal}^2 as follows.

$$p_2(Y_t) = \frac{v(Y_t)}{\sum_{j=K}^{K+L} v(Y_t^{(j)}) + v(Y_t)}, \quad p_2(Y_t^{K+i}) = \frac{v(Y_t^{(K+i)})}{\sum_{j=K}^{K+L} v(Y_t^{(j)}) + v(Y_t)}, \ \forall i = 1, ..., L \ (65)$$

For the posterior probability computation, we replace equation (8) in Lemma 4.2 with the following weighted form.

$$\mathbb{P}\{c(x_{\tau}^*, Y_{\tau}) < 0\} \le \beta_{\tau} = p_2(Y_t) + \sum_{i=1}^{L} p_2\left(Y_t^{K+i}\right) \mathbb{I}\left(S_{\tau}^{(K+i)} < 0\right)$$
(66)

It is evident that when $p_2(Y_t) = p_2(Y_t^{K+i}) = 1/(L+1)$, equation (66) degenerates to equation (8). By applying the weighting schemes in equations (65) and (66) to the test and calibration data, the extended method is capable of handling the covariate shift between them. We refer to this extended approach as Weighted Fb-CP.

To demonstrate the Weighted Fb-CP exhibits robustness to the covariate shift, we design experiments to compare the effects of covariate shift between test trajectories and calibration trajectories on the performance and safety of the proposed method. Apart from the method of generating obstacle trajectories, the experimental setup is identical to that of the kinematic vehicle model experiment in Appendix C.1. To obtain obstacle trajectories with different distributions, the obstacles are modeled using the following double integrator model.

$$\begin{bmatrix} p_{x,t+1} \\ p_{y,t+1} \\ v_{x,t+1} \\ v_{y,t+1} \end{bmatrix} = \begin{bmatrix} p_{x,t} + \Delta v_{x,t} + \frac{\Delta^2}{2} a_{x,t} \\ p_{y,t} + \Delta v_{y,t} + \frac{\Delta^2}{2} a_{y,t} \\ v_{x,t} + \Delta a_{x,t} \\ v_{y,t} + \Delta a_{y,t} \end{bmatrix} + \omega_t e$$
(67)

where (p_x, p_y, v_x, v_y) is the state of an obstacle, consisting of its center of mass and velocity vector. The control input $u=(a_x,a_y)$ is the acceleration vector. Similarly, the sampling time Δ is selected as 0.125. The obstacle trajectories from a given start point to the target point are obtained by solving an optimization problem. ω_t is sampled from a zero-mean Gaussian distribution, with its variance determined by the current state (p_x, p_y, v_x, v_y) . The initial states of the trajectories in the test dataset are sampled from a Gaussian distribution with mean $(-5, 0, 0, 0)^T$, while the initial states of the trajectories in the calibration dataset are sampled from a Gaussian distribution with mean $(0, -5, 0, 0)^T$. As a result, there exists a distribution shift between the trajectories in the test dataset and the calibration dataset. We conducted 1,000 Monte Carlo experiments in this scenario to compare the Weighted Fb-CP, Fb-CP, S-CP Lindemann et al. [2023], and ACI-MP Dixit et al. [2023].

Table 10: Average cost, computation time, and collision avoidance rate using the kinematic vehicle model with different methods ($\alpha = 0.2$).

| | ACI-MP | S-CP | Fb- | -CP | Weighte | d Fb-CP | | |
|--------------------------|--------|-------|-------|-------|---------|--|--|--|
| | | | ARA | IRA | ARA | Weighted Fb-CP ARA IRA 16.27 13.72 84.6% 83.4% | | |
| Average cost | 19.27 | 17.56 | 14.35 | 11.37 | 16.27 | 13.72 | | |
| Collision avoidance rate | 84.8% | 78.7% | 78.6% | 76.8% | 84.6% | 83.4% | | |

Table 10 shows the average cost and collision avoidance rate of 1,000 simulations using the kinematic vehicle model with different methods. It can be observed that due to the covariate shift, both the S-CP and the proposed Fb-CP methods exceed the specified risk tolerance ($\alpha=0.2$). Owing to the reweighting of the test and calibration data, the Weighted Fb-CP method is able to maintain the

collision probability within the prescribed risk tolerance, accompanied by a justifiable and expected increase in average cost. For ACI-MP, since it does not rely on the calibration set, it naturally does not exceed the risk tolerance. However, precisely because it cannot leverage the information contained in the calibration dataset, its average cost is 40.5% higher than that of Weighted Fb-CP-IRA. In summary, we empirically demonstrate that the Weighted Fb-CP is capable of maintaining the risk probability below the specified tolerance under covariate shift, while also achieving a favorable trade-off in terms of average cost.

H Details about the prediction regions

In this Section, we investigate the impact of using prior versus posterior probabilities on the prediction regions. To this end, we collect the prediction region radius for time t, denoted as $C_{20|t}$, using the vehicle model with different methods across 1,000 simulations, as illustrated in Figure 3. It can be observed that $C_{20|t}$ decreases as t increases, which is reasonable since the error of the trajectory predictor diminishes as t approaches τ . Note that since S-CP only uses prior probabilities to compute $C_{20|t}$ throughout the entire planning process, which depends solely on D_{cal} , $C_{20|t}$ remains constant for a fixed t. By contrast, for Fb-CP-ARA, $C_{20|t}$ also depends on the actual obstacle positions and past decisions due to the use of the posterior probabilities, which leads to the variability of $C_{20|t}$ across 1,000 simulations. The distribution of $C_{20|9}$ is shown in the right panel of Figure 3. It can be seen that $C_{20|t}$ computed by Fb-CP-ARA is typically smaller than that computed by S-CP. As t increases, more posterior probabilities can be used, leading to a growing gap between the $C_{20|t}$ calculated by the two methods, which corroborates Corollary A.2.

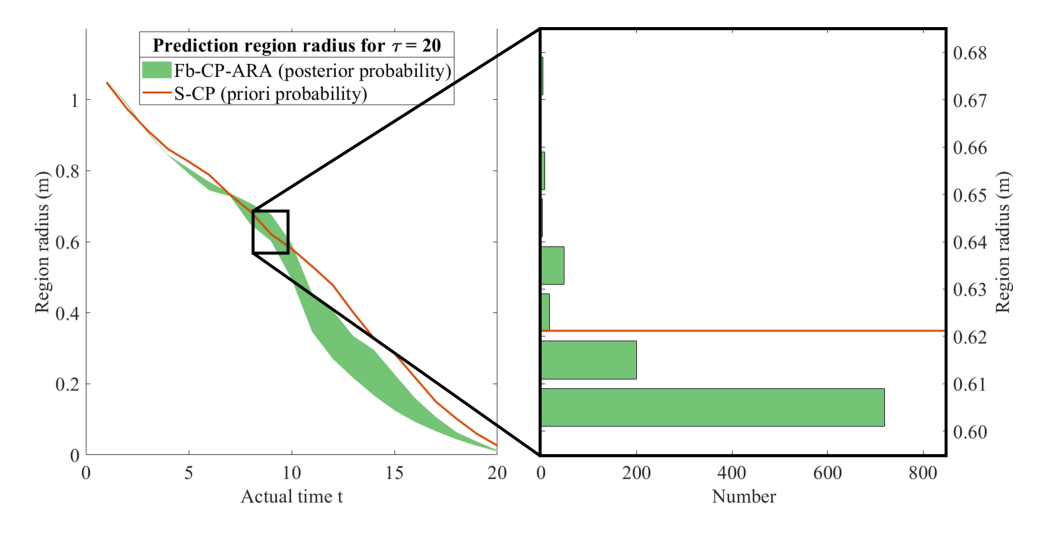


Figure 3: Left: prediction region radius for $\tau=20$ at each time t ($C_{20|t}$) using the vehicle model with different methods across 1,000 simulations. Right: distributions of $C_{20|9}$.

Furthermore, Table 11 shows the prediction region radius for different time t and τ ($C_{\tau|t}$). At the initial state (t=0), no realized state is available for calculating posterior probabilities. As a result, $C_{\tau|0}$ for all τ obtained by S-CP and Fb-CP-ARA are essentially identical, with minor differences arising from the fact that S-CP utilizes the calibration \mathcal{D}_{cal} , whereas Fb-CP-ARA only employs \mathcal{D}_{cal}^1 . As the system operates, an increasing number of realized states x_t^* are available for the calculation of posterior probabilities, enabling Fb-CP to yield a relatively narrower prediction region, corresponding to a smaller $C_{\tau|t}$. As shown in Table 11, the average ratio of the predicted region radius obtained by Fb-CP-ARA to those by S-CP generally exhibits a decreasing trend as time t increases. Moreover, when t>10, based on sufficient posterior probabilities, the prediction region radius obtained by Fb-CP-ARA is reduced by more than 50% compared to that of S-CP.

Table 11: Prediction region radius for different τ and t ($C_{\tau|t}$) using the kinematic vehicle model with different methods (S-CP and Fb-CP-ARA) across 1,000 simulations ($\alpha = 0.2$).

| , | | $\tau = 3$ | $\tau = 6$ | $\tau = 9$ | $\tau = 12$ | $\tau = 15$ | $\tau = 18$ | Ratio |
|--------|-------------------|------------------|------------------|------------------|------------------|------------------|------------------|-------|
| t = 0 | Fb-CP-ARA S-CP | $0.125 \\ 0.129$ | $0.258 \\ 0.247$ | $0.374 \\ 0.374$ | $0.519 \\ 0.520$ | $0.698 \\ 0.691$ | $0.913 \\ 0.902$ | 1.005 |
| t=3 | Fb-CP-ARA S-CP | | $0.102 \\ 0.129$ | $0.216 \\ 0.263$ | $0.351 \\ 0.409$ | $0.527 \\ 0.598$ | $0.705 \\ 0.738$ | 0.793 |
| t = 6 | Fb-CP-ARA S-CP | \ | \ | $0.141 \\ 0.152$ | $0.289 \\ 0.304$ | $0.442 \\ 0.451$ | $0.604 \\ 0.625$ | 0.956 |
| t = 9 | Fb-CP-ARA S-CP | \ | \ | \ | $0.134 \\ 0.149$ | $0.268 \\ 0.305$ | $0.414 \\ 0.466$ | 0.889 |
| t = 12 | Fb-CP-ARA S-CP | | _ | _ | _ | $0.059 \\ 0.138$ | $0.139 \\ 0.291$ | 0.453 |
| t = 15 | Fb-CP-ARA S-CP | | | | _ | _ | $0.054 \\ 0.115$ | 0.470 |

I Computation time of IRA and the hybrid method of ARA and IRA

Table 12 shows the average computation time at each time t using the kinematic vehicle model with Fb-CP-IRA ($\alpha=0.2$). It can be observed that, in practice, the majority of the additional computational burden introduced by IRA arises at the initial time t=0, where it is used to obtain the initial risk allocation and initial trajectory. At subsequent time steps, by using the optimal solution from the previous time step (or iteration) as the initial value for the next time step (or iteration), the IRA algorithm can converge quickly. It is important to note that the TO problem at the initial time step can be solved offline, while the average computation time for TO at subsequent time steps is much smaller than the sampling time (0.125s). Therefore, Fb-CP-IRA is well-suited for real-time TO.

Table 12: Average Computation Time (ACT) at each time t using the kinematic vehicle model with Fb-CP-IRA ($\alpha=0.2$).

| t | 0 | 1 | 2 | 3 | 4 | 5 | 6 | 7 | 8 | 9 |
|------------------------|-------------|-------------|-------|-------------|-------|-------------|-------|-------|-------------|-------------|
| ACT | 2.302 | 0.035 | 0.033 | 0.032 | 0.028 | 0.026 | 0.024 | 0.022 | 0.021 | 0.022 |
| $\frac{t}{\text{ACT}}$ | 10 0.015 | 11 0.011 | | 13 0.009 | | 15 0.007 | - 0 | -, | 18 0.005 | 19 0.002 |

Furthermore, we explore a hybrid method of ARA and IRA to achieve a trade-off between average cost and average computation time. Specifically, we define a switching time t_s , such that when $t < t_s$, the IRA method is used, and when $t \ge t_s$, the ARA method is applied. Table 13 shows the average cost and computation time using the kinematic vehicle model with different switching time t_s ($\alpha=0.2$). It can be observed that using IRA only at the initial time step results in a 66.56% reduction in average cost. This is because the trajectory obtained at the initial time step determines the overall path of the entire trajectory. As t_s increases, the average cost naturally decreases. When t_s reaches 11, further increases in t_s no longer lead to significant reduction in the average cost. This is because, in our scenario, the interaction between obstacles and the vehicle is most intensive at the middle of the mission time. After t>11, the obstacles and the vehicle have moved apart, significantly reducing the collision risk, which results in ARA and IRA optimizing nearly identical trajectory. Although the aforementioned hybrid method balances the trade-off between average cost and computation time, as previously mentioned, executing IRA at the initial time step is the primary source of both cost reduction and increased computation time.

Table 13: Average cost and computation time using the kinematic vehicle model with different switching time t_s ($\alpha = 0.2$).

| t_s | 0 (ARA) | 1 | 6 | 11 | 16 | 20 (IRA) |
|--------------------------|---------|-------|-------|-------|-------|----------|
| Average cost | 15.13 | 5.06 | 3.74 | 2.90 | 2.89 | 2.89 |
| Average computation time | 0.078 | 0.118 | 0.121 | 0.129 | 0.129 | 0.131 |

J Sensitivity analysis of the calibration set division

Table 14 shows the average cost, average computation time and collision avoidance rate using the kinematic vehicle model and Fb-CP-ARA ($\alpha=0.2$) with 10 different random calibration set divisions. Specifically, for each experiment, we randomly divide the calibration dataset D_{cal} into D_{cal}^1 and D_{cal}^2 . It can be observed that, for the ten random experiments, the standard deviation of the average cost is 0.643, and the coefficient of variation is 4.2%, indicating relatively low volatility. For the collision avoidance rate, its volatility is only 2.3%, and all values do not exceed the given tolerance (80%). Therefore, the proposed method is insensitive to the calibration set division.

Table 14: Average Cost (AC), Average Computation Time (ACT) and Collision Avoidance Rate (CAR) using the kinematic vehicle model and Fb-CP-ARA ($\alpha=0.2$) with 10 different random calibration set divisions.

| Index | 1 | 2 | 3 | 4 | 5 | 6 | 7 | 8 | 9 | 10 |
|-------|-------|-------|-------|-------|-------|-------|-------|-------|-------|-------|
| AC | 15.13 | 14.78 | 15.11 | 16.03 | 15.96 | 14.37 | 14.60 | 15.73 | 15.64 | 16.19 |
| ACT | 0.078 | 0.078 | 0.079 | 0.077 | 0.072 | 0.080 | 0.065 | 0.074 | 0.086 | 0.084 |
| CAR | 89.1% | 89.2% | 90.5% | 88.2% | 88.6% | 88.4% | 90.5% | 89.2% | 89.3% | 89.9% |

K An extension using the normalized nonconformity score

Stamouli et al. [2024] proposed a normalized nonconformity score, which can improve performance compared to S-CP [Lindemann et al., 2023]. In this section, we incorporate this normalized nonconformity score into Fb-CP to further enhance its performance as follows. First, we still follow the content outlined prior to Section 4.1. Instead of using the original nonconformity score as in Section 4.1, we can redefine the nonconformity score at time τ as follows to replace (5).

$$R_{\tau} = \max_{t=0,...,\tau-1} \left\{ \frac{\|Y_{\tau} - \hat{Y}_{\tau|t}\|}{\sigma_{\tau|t}} \right\}$$

$$R_{\tau}^{(i)} = \max_{t=0,...,\tau-1} \left\{ \frac{\|Y_{\tau}^{(i)} - \hat{Y}_{\tau|t}^{(i)}\|}{\sigma_{\tau|t}} \right\} \quad \forall i = 1,...,K$$

$$(68)$$

where

$$\sigma_{\tau|t} = \max_{j \in \mathcal{I}_{train}} \|Y_{\tau}^{(j)} - \hat{Y}_{\tau|t}^{(j)}\|, \quad \forall t, \ \tau > t$$
 (69)

where $\mathcal{I}_{train} = \{j: Y^{(j)} \in D_{train}\}$ denotes the set of indices of the data in the training set D_{train} . We note that, compared to the nonconformity score in Stamouli et al. [2024], we separate the nonconformity score at each time τ , which facilitates the reallocation of the risk at each time step. Similarly, given an allocated risk α_{τ} for future time τ , the random variables $R_{\tau}, R_{\tau}^{(1)}, ..., R_{\tau}^{(K)}$ are exchangeable and the prediction region with coverage guarantee is derived as follows.

$$\mathbb{P}\left\{\max_{t=0,\dots,\tau-1}\left\{\frac{\|Y_{\tau}-\hat{Y}_{\tau|t}\|}{\sigma_{\tau|t}}\right\} \le C_{\tau}^{1-\alpha_{\tau}}\right\} \ge 1-\alpha_{\tau} \tag{70a}$$

$$C_{\tau}^{1-\alpha_{\tau}} = Quantile_{1-\alpha_{\tau}}(R_{\tau}^{(1)}, ..., R_{\tau}^{(K)}, \infty)$$

$$\tag{70b}$$

Based on the $(1 - \alpha_{\tau})$ -coverage prediction region defined in (70a), the individual chance constraint $\mathbb{P}\left\{c(x_{\tau}, Y_{\tau}) \geq 0\right\} \geq 1 - \alpha_{\tau}$ can be reformulated as the following lemma.

Lemma K.1 (chance constraint) If Assumption 3.1 holds, the constraint function c is L-Lipschitz continuous and $\max_{0 \le s \le t} \{c(x_\tau, \hat{Y}_{\tau|t}) - LC_{\tau|t}^{1-\alpha_\tau}\} \ge 0$ is satisfied where $C_{\tau|t}^{1-\alpha_\tau} = \sigma_{\tau|t}C_{\tau}^{1-\alpha_\tau}$, then the individual chance constraint $\mathbb{P}\{c(x_\tau, Y_\tau) \ge 0\} \ge 1 - \alpha_\tau$ is satisfied.

Proof: According to the $(1 - \alpha_{\tau})$ -coverage prediction region defined in 70a, we can obtain that

$$\mathbb{P}\left\{\bigcap_{t=0}^{\tau-1} \left\{ \frac{\|Y_{\tau} - \hat{Y}_{\tau|t}\|}{\sigma_{\tau|t}} \right\} \le C_{\tau}^{1-\alpha_{\tau}} \right\} \ge 1 - \alpha_{\tau} \tag{71}$$

According to that fact $t \leq \tau - 1$ and the definition, we have the following inequality.

$$\mathbb{P}\left\{\bigcap_{t=0}^{t} \left\{ \|Y_{\tau} - \hat{Y}_{\tau|t}\| - C_{\tau|t}^{1-\alpha_{\tau}} \right\} \le 0 \right\} \ge \mathbb{P}\left\{\bigcap_{t=0}^{\tau-1} \left\{ \|Y_{\tau} - \hat{Y}_{\tau|t}\| - C_{\tau|t}^{1-\alpha_{\tau}} \right\} \le 0 \right\} \ge 1 - \alpha_{\tau} \tag{72}$$

Based on (72), we can further obtain the following inequality.

$$\mathbb{P}\left\{C_{\tau|s}^{1-\alpha_{\tau}} - \|Y_{\tau} - \hat{Y}_{\tau|s}\| \ge 0\right\} \ge 1 - \alpha_{\tau}, \quad \forall s = 0, ..., t$$
(73)

Note that the function c is L-Lipschitz continuous, the following inequality is obtained.

$$||c(x_{\tau}, Y_{\tau}) - c(x_{\tau}, \hat{Y}_{\tau|t})|| \le L||Y_{\tau} - \hat{Y}_{\tau|t}|| \Longrightarrow c(x_{\tau}, Y_{\tau}) \ge c(x_{\tau}, \hat{Y}_{\tau|t}) - L||Y_{\tau} - \hat{Y}_{\tau|t}||$$
 (74)

If the constraint $\max_{0 \le s \le t} \{c(x_{\tau}, \hat{Y}_{\tau|t}) - LC_{\tau|t}^{1-\alpha_{\tau}}\} \ge 0$ is satisfied, we have the following inequality.

$$\exists s = 0, ..., t \quad c(x_{\tau}, Y_{\tau}) \ge L(C_{\tau|s}^{1-\alpha_{\tau}} - ||Y_{\tau} - \hat{Y}_{\tau|s}||)$$
(75)

By combining (73) and (75), we ultimately obtain $\mathbb{P}\{c(x_{\tau}, Y_{\tau}) \geq 0\} \geq 1 - \alpha_{\tau}$.

Finally, it is sufficient to replace constraint (11e) in the TO problem (11) with $\max_{0 \leq s \leq t} \{c(x_{\tau}, \hat{Y}_{\tau|t}) - LC_{\tau|t}^{1-\alpha_{\tau}}\} \geq 0$. For the posterior probability calculation and risk allocation method, since we have separated the nonconformity score at each time step τ , our proposed framework remains fully applicable. It is important to note that, as described in Section C, the constraint $\max_{0 \leq s \leq t} \{c(x_{\tau}, \hat{Y}_{\tau|t}) - LC_{\tau|t}^{1-\alpha_{\tau}}\} \geq 0$ introduces mixed-integer variables into the TO problem, which significantly increases the solution time, especially when using the IRA method and dealing with nonlinear systems.

L Limitations

The main limitation lies in the reliance of the proposed method on the size of the calibration dataset. As previously mentioned, to ensure coverage guarantees within the closed-loop framework, the calibration dataset needs to be split into two parts: one for forward computation of prediction regions and the other for backward computation of posterior probabilities. This requirement results in the proposed method needing a larger calibration dataset compared to standard CP methods. However, extensive data can be sourced from advanced high-fidelity simulators or robotic applications like autonomous vehicles, where datasets are increasingly accessible. Thus we believe that the reliance on data quantity will not present a substantial challenge.

M Broader Impacts

This work proposes a novel Fb-CP framework for trajectory optimization under uncertainty, with provable safety guarantees and adaptive risk control. The method has potential positive societal impacts on safety-critical applications such as autonomous vehicles, robotics, and disaster response, by improving the reliability and efficiency of decision-making under uncertainty. It also contributes to the development of trustworthy AI through its theoretical guarantees and feedback-based adaptability.

However, potential negative societal impacts include misuse in high-risk or adversarial settings (e.g., autonomous weapons), privacy concerns from trajectory data collection, and overconfident decisions if the system fails under distribution shift. To mitigate these risks, future deployments should incorporate rigorous validation, privacy safeguards, and oversight mechanisms to ensure safe and ethical use of the proposed method.